STUDIA

UNIVERSITATIS BABEŞ-BOLYAI

PHYSICA

(40)1

1995

CLUJ-NAPOCA

Anul XL 1995

STUDIA
UNIVERSITATIS BABEŞ-BOLYAI

PHYSICA

1

Editorial Office: 3400 CLUJ-NAPOCA str. M Kogălniceanu nr 1 ▸ Telefon 194315

SUMAR - CONTENTS - SOMMAIRE

Theoretical Physics

Chronicle

STUDIA UNIV BABEŞ-BOLYAI, PHYSICA, XL, 1, 1995

RAMAN, IR AND SERS STUDIES OF 2,4-DIAMINO-6-PHENYL-1,3,5-TRIAZINE

S. CÎNTA[1,2], T. ILIESCU[1], M. VLASSA[3], M. VENTER[3], I. MARIAN[3] and I.Beldeanu[3]

ABSTRACT. - Preliminaries studies on 2,4-Diamino-6-Phenyl-1,3,5-Triazine (DAFT) were made, using Raman, IR and SERS spectroscopy.

One protonated form of DAFT molecule was putted in evidence from the two forms theoretically expected The orientation of DAFT molecule and the DAFT-ion adsorbed on silver surface was established by comparison of Raman and SERS spectra

Introduction

Surface-enhanced Raman scattering (SERS) is now an well established technique in order to investigate physical and chemical interactions between an adsorbate molecule and the metal surface

Molecules containing one nitrogen atom in aromatic ring, like pyridine and its derivatives were largely studied in this field [1]

But there are very few SERS studies over the molecules containing two or three nitrogen atoms in aromatic ring [2-6]

In this paper we present our Raman, IR and SERS preliminar investigations over DAFT molecule in order to draw conclusions about its protonated forms and configurations adsorbed on silver sol

Our study of DAFT intends to put in evidence whether this molecule presents two different protonated forms which the theory predicts and whether both of them adsorbs on the

[1] Corresponding author

[2] *"Babeş-Bolyai" University, Faculty of Physics, 3400 Cluj-Napoca, Romania*

[3] *"Babeş-Bolyai" University, Faculty of Chemistry, 3400 Cluj-Napoca, Romania*

silver surface

Experimental

DAFT was purchased from Aldrich and was used without other purification

Silver sol was prepared by the process described by Creighton et all [7] For the freshly prepared sol the molar ratio $NaBH_4$ $AgNO_3$ was 6 At the experiment time the sol age[8] was about two months

DAFT is a hardly solved compound either in ethanol or in water, in last one, only in the presence of acidic medium

There were used three DAFT solutions one in ethanol and the others two in water with 2 and 5 stoechiometric HCl molar ratio, respectively In all of them DAFT concentration was 10^{-1}M and the hydrochloric acid concentration in aqueous solutions was $2x10^{-1}$M and $5x10^{-1}$M respectively

The Raman spectra were recorded with a double monochromator GDM-1000 using the 488 nm excitation line from an argon ion laser The spectral slit width was 4 cm^{-1}, the laser power 140mW and the wavenumbers for all bands are accurate to ± 4 cm^{-1}

The samples were introduced into a capillary glass tube and the scattered light was collected at right angle

Each SERS-active systems were obtained using 1 ml silver sol and 0,05 ml of each DAFT solution The final DAFT concentration in sample was $4,7x10^{-3}$M

Infrared spectra of solid DAFT and recrystalised DAFT-ions were recorded with a UR20 Carl Zeiss spectrophotometer in the 400-4000 cm^{-1} spectral range, using the KBr pellet technique

All spectra, excepting that one marked in figure legend, were recorded at room temperature

The chemicals were reagent grade and triply distilled water was used throughout

Results and Discussion

In solid powder, DAFT is a very scattering compound, so Raman spectrum, showed in Fig 1 a) was easily obtained

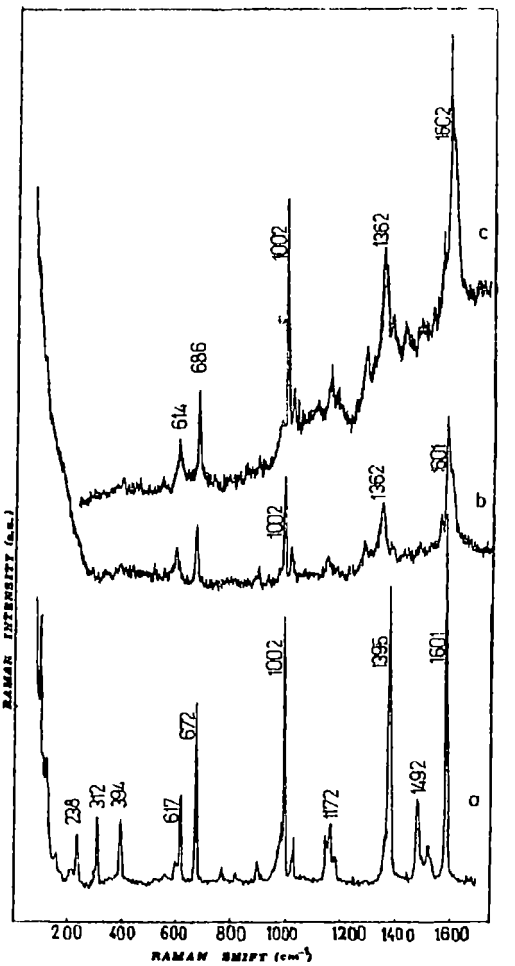

Fig.1. Raman spectra of solid DAFT a), DAFT-aqueous solutions at pH=1 75 (b) and pH=0 75 (c) respectively (c- spectrum was obtained at 60°C, see text)

Fig 1 b) and c) show Raman spectra of aqueous solutions containing 1 2 and 1 5 molar ratio DAFT HCl respectively, with pH values at 1 75 and 0 75

Fig 2 shows the theoretically changes in the structure of DAFT with pH variation

The tautomeric possible states in 4,6-diamino-2-phenyl-1,3,5-triazine are indicated in the structures I-IV The two mono-imino forms (II and III) are twice as likely of being the more probable structures of the compound because only one diamino and only one di-imino structures can be formulated (I and IV) This may also account for the fact that only monohydrochlorides are formed in this type[9]

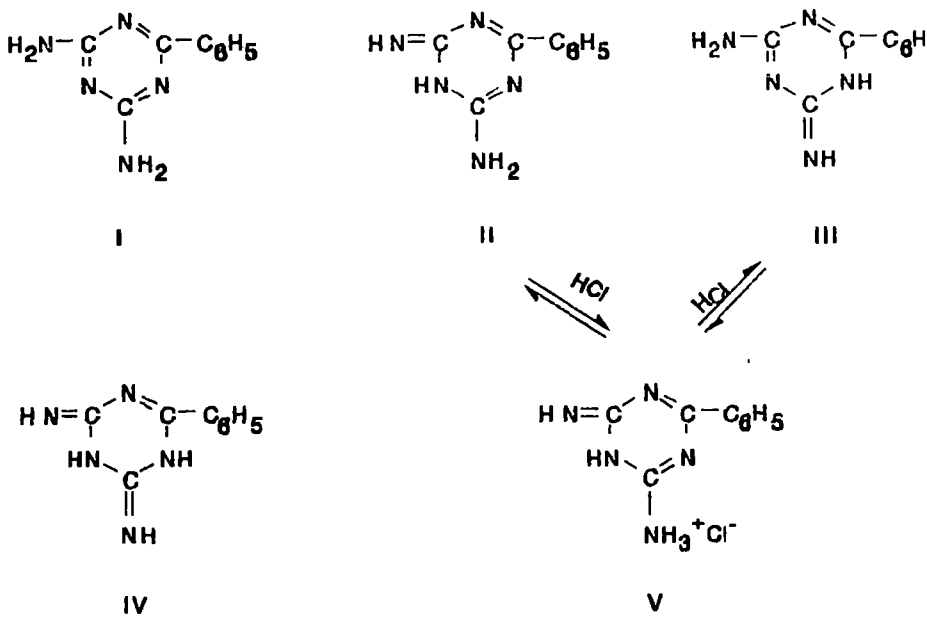

Fig.2. The structural change of DAFT with variation of pH

On passing to very strong acidic medium (pH<1) a marked batho- and hypochromic shift is to be observed[10] which indicates that the degree of conjugation is diminished The shifting could be interpreted as the result of a favoring of structure IV in strongly acidic solution as the preferential form However in the crystallization of the hydrochloride, the more probable forms II and III are predominant[9]

The ethanol solution of DAFT presents a strong fluorescence which makes impossibly getting the Raman spectrum, but allows a very good SERS spectrum (fig 3 a) Assumming that DAFT-ethanol solution keeps the neutral form of the molecule, its SERS spectrum proves that neutral DAFT is adsorbed on the silver surface

Fig 4 shows the IR spectra a) for neutral DAFT and b) for solid DAFT-ion (V)

If we consider the molecule as a whole, the total number of normal vibrations will be 63 Since the identification of all the normal modes of such a big molecule is not an easy task, from the very begining of the vibrational study, we consider the molecule as 3-

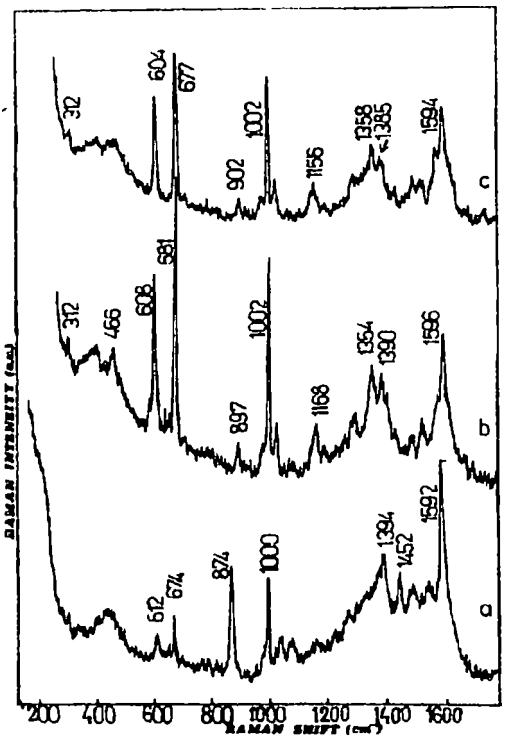

Fig.3. SERS spectra of DAFT-ethanol solution a), DAFT-aqueous solution I (b) and II (c) respectively

substituted triazine, where the substituent groups are amino (double) and phenyl

When the amino group is participating in hydrogen bounding, the position of the lower frequency band is fairly constant

Comparing the peaks position of neutral DAFT Raman spectrum with that of 1,3,5-Triazine[11,12,13], we can assign 1492* and 1395 peaks as triazinic ring stretching vibrations

While the interactions between the triazine ring and phenyl are considered, some of the ring modes are expected to split into two components The magnitude of the splitting will depend on the strengths of interaction between two rings

On the other hand, concerning the influence of the amino double group, in the 3500-3300 N-H stretching frequency region from the IR spectrum a), three large bands develop and

* All frequencies in cm-1

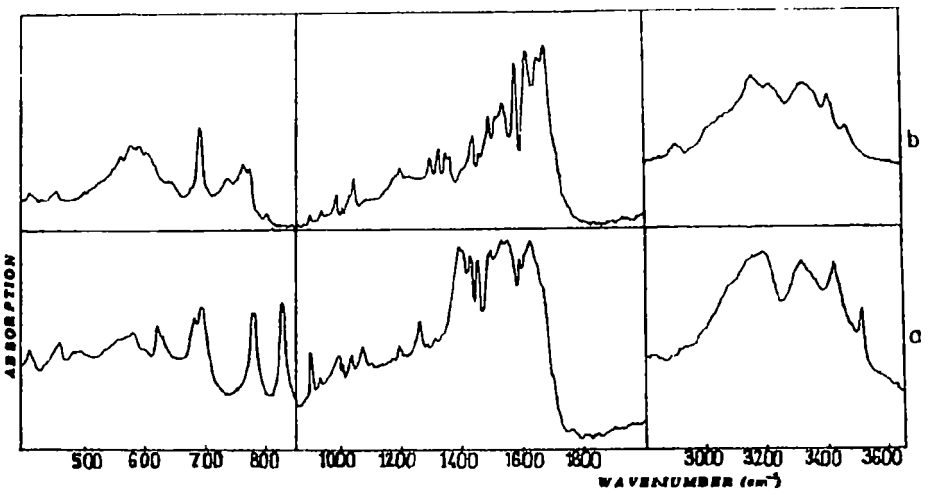

Fig.4. IR spectra of solid DAFT (a) and solid DAFT-ion V (b)

this is an indication that the orientation of the N-H bond in the amino group is such that there exists some intra-molecular hydrogen bond between the -NH_2 group and the lone pair of the triazinic nitrogen atoms

Comparing a),b) and c) Raman spectra (see Fig 1), the peak from 1601 keeps constant position in the both solution spectra and is assigned as phenyl ring stretching mode

The lower frequency shifted peak from 1395 in neutral DAFT to 1362 in both solutions, is due to proton attachement to the nitrogen atom from -NH_2 group to give -NH_3^+ rather than to the ring's nitrogen (forming N-H^+)

If the -NH_3^+ groups result, the C-N bond (to amine) lenght will increase , so N-C-N symmetric stretching frequency shifts to lower position

The strong Raman band in neutral and protonated DAFT form from 1002, remaining constantly in all spectra, is undoubtedly due to the Raman active symmetrical N-C-N ring stretching vibration

The background of this peak shows an overlapping with in plan C-H bending phenyl modes

Out of plane phenyl-ring bending modes appear at 822, 767, 672, 617, 394 in Raman and at 826, 775, 690, 680 and 620 in IR spectrum On the other hand, NH2 group presents wagging modes in the 800-600 IR spectral range Comparing a) and b) IR spectra (see Fig 3) the great modifications which appear, demonstrate the existence of the V-protonated specia

The SERS spectra are showed in Fig 3 a)-the neutral DAFT ethanol solution, b) V-DAFT-ion aqueous solution and c) IV DAFT aqueous solution

Variations in the SERS spectra with change in the bulk pH were usually attributed either to a change in orientation of adsorbates molecules with respect to the metal surface or to a change in its chemical nature[14,15]

For aromatic molecules it has generally been known[16] that the frequencies of ring stretching vibrations decrease or red shift by more that 10 cm^{-1} and their band increase substantially when the molecules adsorb on the metal surface via their π systems

Comparing a), b) and c) SERS spectra, DAFT and V DAFT-ion species are less adsorbed via their π ring system

Comparing a) and b) SERS spectra, the 1394 peak belonging to NH_2 group has a double correspondence in b) spectrum, to 1390 and 1354

This might be an evidence that in first DAFT aqueous solution (pH=1,75) dropped on the silver sol, both neutral and protonated specia of DAFT can exist

At a lower pH (c) SERS spectrum), the protonated DAFT mainly exists (the 1358 peak higher than 1385)

Between b) and c) SERS spectra, the small differences which can be observed can not be responsable for change in orientation of the adsorbate (our supposition)

Big changes are observed in the intensity of 608 and 681 peaks (b) SERS spectrum), 604, 677 (c) SERS spectrum) compared with the correspondents 612, 674 from a) spectrum

Moreover 874 peak from a) is esentially decreased in b) and c) Concerning this

comparison, might be an evidence that both neutral DAFT and V DAFT-ion are adsorbed on the silver surface mainly through the lone pair electrons of the nitrogen atoms from the "background" of the molecule one from the triazine ring and the others from NH_2 groups and NH_3^+, respectively

Further investigations over the change in orientation of this species with pH variation are in progress

REFERENCES

1 Surface-Enhanced Raman Scattering, eds K R Chang and T E Furtak, Plenum Press, New York, 1982
2 F. Zhong, G. Wu, J. Molec Structure, 324, 233 (1994)
3 B Tian, G Wu and G Liu, J. Chem Phys, 87, 7300 (1987).
4 Y Huang and G Wu, Spectrochim Acta, Part A, 46, 337 (1990)
5 G. Wu, J Molec Structure, 238, 79 (1990)
6 E J Liang, D Göttges and W Kiefer, Applied Spectroscopy, vol 48, nr 9 1088 (1994)
7 J A Creighton, C G Blatchford and M G Albrecht, J. Chem. Soc. Faraday Trans. II, 75, 790 (1979)
8 K Cermákova, O Šesták, P Matejka, V Baumruk, B Vlckova, Collect Czech. Chem Commun, 58, 2682 (1993)
9 A Ostrogovich, G Gheorghiu, Gazz chim. ital, 60, 648 (1930)
10 F Nachod, E Steck, J Amer Chem Soc, 70, 2818, 1948
11 W M Padgett, H and W M Hammer, J.Am Chem.Soc, 80, 803 (1958)
12 H K Reimschussel and N J McDevitt, J Am Chem Soc, 82, 3756 (1960).
13 J E Lancaster and N B Colthup, J Chem.Phys., 22, 1149 (1954)
14 D J Rogers, S D Luck, D E Irish, D.A Guzonas, G F Atkinson, J. Electroanal Chem, 167, 237, (1984)
15 S C Sun, J Bernard, R L Birk, J R Lombardi, J. Electroanal Chem, 196, 359 (1985)
16 P Gao, M Weaver, J Phys Chem., 89, 5040 (1985)

STUDIA UNIV BABEŞ-BOLYAI, PHYSICA, XL, 1, 1995

NMR OBSERVATION OF THE PROTON SPIN-LATTICE RELAXATION IN THE POLYISOPROPENE-TOLUENE SOLUTIONS

M. TODICĂ[1], G. DAMIAN[1], D. CIURCHEA[1] and A.V. POP[1]

ABSTRACT. - Spin-lattice relaxation time T_1 of the protons was measured in deuterated polyisoprene-toluene solutions The temperature dependence of T_1 was analyzed over a wide temperature range above the glass transition temperature T_g for each solution

A superposition property $T_1 = f(T-T_g(\Phi))$ was observed for concentrated solutions This property was connected with the polymer - solvent interaction and with the local mobility of the polymeric chain

Introduction. This work deals with the NMR observation of local chain motions occurring in the polyisoprene-toluene solutions Local dynamics, which refer a few monomer units, strongly depend on the details of the monomer structure

On the other hand, the local dynamics are the bases of the complex dynamics of polymeric chains, like the diffusional translation or reptation [1] Therefore, the information about local dynamics provides an important intermediate link between molecular structure and larger motions

Dynamics on the scale of a few monomer units are intimately connected with the main glass transition in many polymers [2] Certain types of local dynamics can also directly influence the material properties in the sub-T_g region

In polymeric solutions the coupling between the solvent molecules and the monomeric units can affect the local dynamics of the polymeric chain This interaction occurs on such a short length scale and fast time scale that the effect of the solvent on the chain motion cannot be simply represented by the macroscopic viscosity That's why many techniques including NMR and optical measurement were used to investigate the local dynamics [3],[4]

The ^{13}C NMR studies reported on dilute solutions show that the specific interaction

[1] *"Babeş-Bolyai" University, Faculty of Physics, 3400 Cluj-Napoca, Romania*

between polyisoprene and many solvents do not determine the rate or the mechanism of the local polymer motions [5] Furthermore, the local dynamics of polyisoprene vary with the temperature and the viscosity but do not depend upon the solvent identity [5]

In this work we were interested to observe the spin-lattice relaxation of the protons in the polyisoprene-toluene concentrated solutions We correlated these observations with the local dynamics of the polymeric chain

Experimental. NMR measurements were made on 100%, 94%, 78% and 58% solutions of polyisoprene in toluene-d_8 in the temperature range 234 K - 350 K The isomeric conformation of the polyisoprene sample was 92% cis-1,4 The polymeric sample was supplied and characterized by the Manufacture des Pneumatiques Michelin (France) and the toluene-d_8 was purchased from Spectrometrie Spin et Techniques (France) The solutions were enclosed in NMR tubes (diameter 8 mm), sealed under a primary vacuum The concentrations of the solutions were controlled with an accuracy better than 1%

Spin-lattice relaxation times T_1 of the protons were measured using an inversion-recovery sequence (π - τ - $\pi/2$) The values of the relaxation time were obtained by fitting the experimental data with a single exponential function The values of T_1 could be obtained within an accuracy of 10% by performing several measurements The sample temperature was controlled within 1 K All the measurements were performed at 45 MHz, using a CXP Bruker spectrometer

The arrangement of the atoms in the cis-1,4 monomeric unit is

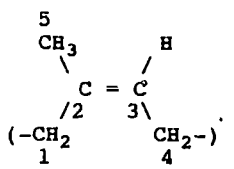

Results and discussions. In the case of molten polymers, the dominant mechanism which govern the proton spin relaxation is the dipole-dipole interaction established between nuclear spins located within one given chain segment The dipole-dipole interaction established between nuclear spins located on different chain segments may also contribute to the spin-lattice relaxation process For this reason we assume that the relaxation time T_1 should be sensitive to the local dynamics of the polymeric chain However, it is difficult to separate the contribution of each type of interaction in the spin relaxation mechanism This problem may be overcome by using the spectral density function J(ω) to describe the spin-lattice relaxation mechanism.

The spin-lattice relaxation rate may be expressed as [6]

$$\frac{1}{T_1} = K \cdot n \cdot [J(\omega_H - \omega_C) + 3 \cdot J(\omega_C) + 6 \cdot J(\omega_H + \omega_C)] \qquad (1)$$

where. ω_C and ω_H are resonance frequencies for carbon and hydrogen, n is the number of the bonded protons The constant K is given by [5]

$$K = \frac{1}{10}\left(\frac{\mu_o \cdot \gamma_H \cdot \gamma_C \cdot \hbar}{4\pi r^3}\right)^2 = 2.15 \cdot 10^9 s^{-2} \qquad (2)$$

where γ_C and γ_H are the gyromagnetic ratios for carbon and hydrogen, r is the C-H bond length (taken 1.09 Å for methene and methylene carbons [7])

The spectral density function J(ω) characterizes the isotropic process of local reorientation and it is related to the autocorrelation function of the spin-spin interaction, G(t) .

$$J(\omega) = \frac{1}{2}\int_{-\infty}^{+\infty} G(t) \cdot e^{i\omega t} \cdot dt \qquad (3)$$

G(t) is expressed as

$$G(t) = \frac{1}{2}\langle 3(\vec{e}_x(0) \cdot \vec{e}_x(t))^2 - 1 \rangle \qquad (4)$$

In this equation, $\vec{e}_x(t)$ is a unit vector in the direction of the C-H bond at the moment t The brackets indicate an assembly average

Often G(t) is not a single exponential and contains a distribution of the correlation time τ, which describes the rotational molecular motion of the C-H bond

When the extreme narrowing condition $(\omega_H+\omega_C)<<1$ is fulfilled for all τ contributing to G(t), Eq (1) simplifies to

$$\frac{1}{T_1} = 10 \cdot n \cdot K \cdot \tau_c \tag{5}$$

We assume that spin-lattice relaxation rates of the protons located in different sides of the monomeric units have different values because their bond lengths are different However, recent works performed on polybutadiene have shown that the relaxation rates of the protons attached to methene or methylene groups are about equal respectively [8] In this case all the protons could be characterized by a single relaxation time T_1

The monomer configurations of the polyisoprene and polybutadiene are not so different and therefore we shall consider here these results We also assume that the dynamics of the molecular processes observed by NMR are governed by a single correlation time τ_c

Both τ_c and T_1 are temperature dependent. The correlation time τ_c is simply related to the Larmor frequency ω_0 at the maximum of the spin-lattice relaxation rate. In this case,

$$\omega_0 \cdot \tau_c \approx 1 \tag{6}$$

which means that the frequency of the local reorientation is equal to the Larmor frequency [9]

The temperature dependence of the relaxation time T_1 for the molten polyisoprene is shown in Fig 1

The minimum value of the spin-lattice relaxation time is T_{1min}=50 ms ± 5 ms corresponding to T=306 K From Eq (6) we calculated the value of the correlation time corresponding to this temperature We found $\tau_c \approx 2.2 \cdot 10^{-8}$s

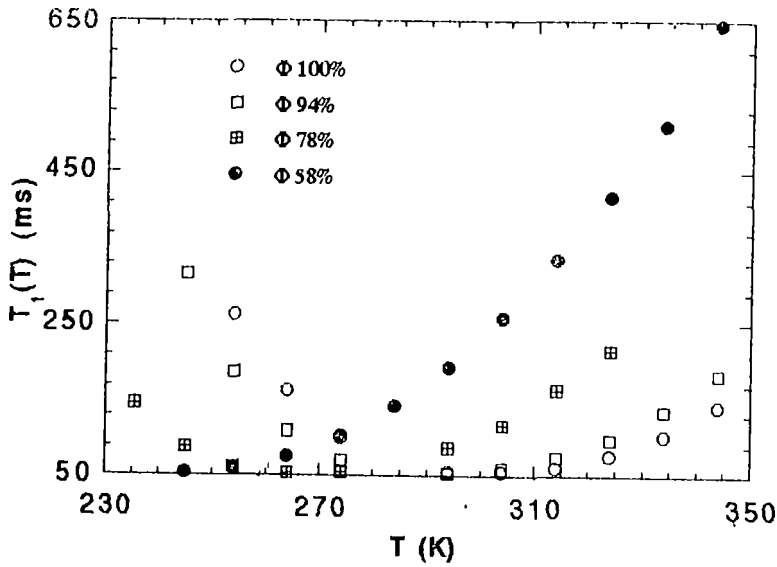

Fig.1. Temperature dependence of the proton spin-lattice relaxation time in polyisoprene-toluene solutions Φ is the polymer concentration

In the case of the polymeric solutions the relaxation time T_1 of the protons may be affected by the dipole-dipole interaction between the polymer and the solvent To verify this hypothesis we measured the relaxation time T_1 for different polymer concentrations Fig 1 also shows the temperature dependence of T_1 for different polyisoprene-toluene solutions

For each sample the minimum of T_1 occurs at a temperature $\Theta(\phi)$ depending on the polymer concentration but the minimum value of the T_1 is the same $T_{1min}(\phi,\Theta)$=50 ms ± 5 ms in all cases This behavior suggests the same relaxation mechanism at the$\Theta(\phi)$ temperature for all samples and does not depend on the solvent concentration

By using Eq (6) we calculated the correlation time $\tau(\phi,\Theta)$ for each concentration at the $\Theta(\phi)$ temperatures We found $\tau(\phi,\Theta)\approx 2.2\cdot 10^{-8} s$, the same as for the molten polymer It results that at any temperature T the local reorientation motion is faster in the dilute

solutions

We observed that the temperature $\Theta(\phi)$ and the glass transition temperature $T_g(\Phi)$ of the solutions have the same concentration dependence, as it is shown in Fig 2

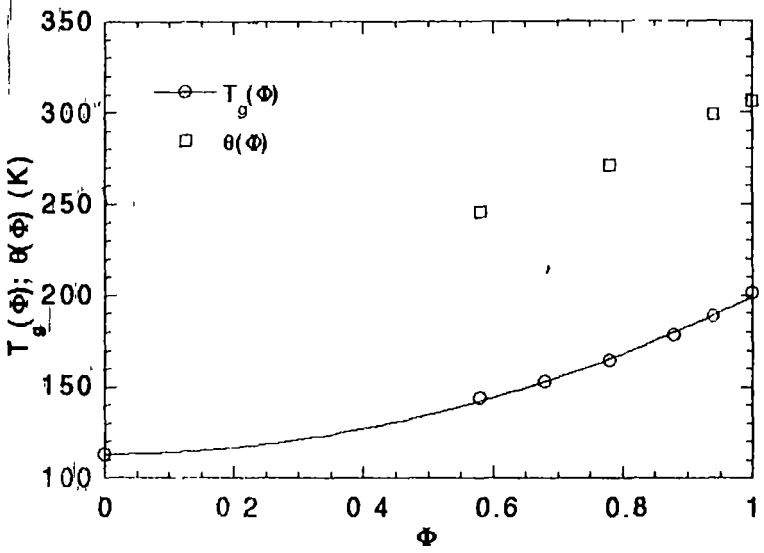

Fig.2. The concentration dependence for the glass transition (T_g) temperature and for the temperature $\Theta(\Phi)$

The glass-transition temperature of the solutions [2] were calculated using the relation

$$T_g(\Phi) = \frac{\alpha_p \cdot T_g^p \cdot \Phi + \alpha_p \cdot T_g^s \cdot (1 - \Phi)}{\alpha_p \cdot \Phi + \alpha_S \cdot (1 - \Phi)} \tag{7}$$

The glass-transition temperatures and the thermal expansion coefficients of the polymer and solvent are [10]

$$\begin{aligned} T_g^p &= 201 \pm 3K \qquad \textit{and} \qquad T_g^s = 113K \\ \alpha_p &= 6.7 \cdot 10^{-4} K^{-1} \qquad \textit{and} \qquad \alpha_s = 1.7 \cdot 10^{-3} K^{-1} \end{aligned} \tag{8}$$

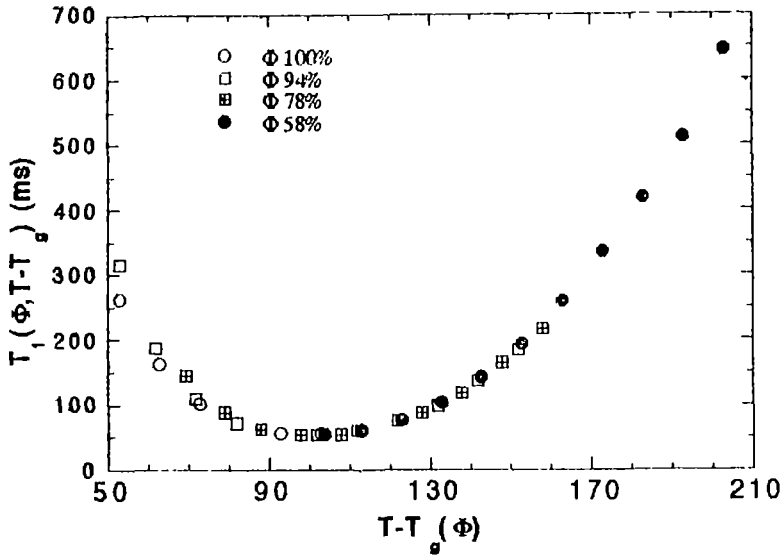

Fig.3. The superposition property of the relaxation time T_1 versus the variable $T-T_g(\Phi)$

We observed that $\Theta(\Phi) - T_g(\Phi) = 107 \pm 4K$ for all the samples This relation suggests a novel representation of the relaxation time T_1 versus a new variable $T-T_g(\Phi)$ In this representation all the $T_1(\Phi,T-T_g(\Phi))$ curves are superposed (Fig 3)

For any concentration Φ, the dependence of the relaxation time T_1 versus the $T-T_g(\Phi)$ variable is the same This means that the spin-lattice relaxation mechanism does not depend on the solvent concentration This result is in agreement with other works [5,11], which shows that the spin-lattice relaxation time of the backbone carbon atoms is the same for both toluene-d_8 and toluene-h_8 used as solvents

Therefore, one may conclude that the dipole-dipole interaction between the spins of the polymeric chain and the solvent is weaker than the interaction between the spins located in the polymeric chain

Concerning the relation between the correlation time τ_c, the solvent concentration and the temperature, we obtained the remarkable result that for any concentration the value

$\tau \approx 2\ 2 \cdot 10^{-8}$s corresponds to a temperature $\Theta(\Phi)=T_g+(107 \pm 4)$ K Thus, the local mobility of the polymeric chain became independent on the solvent concentration at the temperature $\Theta(\Phi)$

Conclusions. The superposition property of the dependence $T_1(\Phi, T-T_g(\Phi))$ versus $T-T_g(\Phi)$ suggests that the mechanism of the spin-lattice relaxation of the protons attached to the polymeric chain in concentrated solutions polyisoprene-toluene does not depend on the solvent concentration

The dipole-dipole interaction between the spins of the polymer and the spins of the solvent spins is weaker than the interaction between the spins of the polymeric chain

When the relaxation time reaches its minimum as a function of temperature,the calculated value of the correlation time is the same $\tau_c=2\ 2 \cdot 10^{-8}$ s, for all solvent concentrations In all cases, this minimum was observed at the temperature $\Theta(\Phi)=T_g+(107 \pm 4)$ K

REFERENCES

[1] P G De Gennes , "Scaling Concepts in Polymer Physics", Cornell University Press, Ithaca, New York, 1979

[2] J Ferry, "Viscoelastic Properties of Polymers, 3rd ed , Wiley, New York, 1980

[3] P D Hyde, M D Edinger, T Kitano, K Ito, Macromolecules, **22**, 2253 (1989)

[4] D B Adolf, M D Edinger, T Kitano, K Ito, Macromolecules, **25**, 867 (1992)

[5] S Glowinkowski, D J Gisser, M D Ediger, Macromolecules, **23**, 3520 (1990)

[6] A Abragam, "Principles of Nuclear Magnetism", Oxford University Press, London, 1961

[7] J A Pople, M Gordan, J Am Chem Soc , **89**, 420 (1967)

[8] A Guillermo, R Dupeyre, Cohen-Addad, J P Macromolecules, **23**, 1291 (1990)

[9] I Ya Slonim, A N Lyubimov, "The NMR of Polymers", Plenum Press, New York, 1970

[10] J Brandrup, E H Immergut, Editors, Polymer Handbook, 2nd ed , John Wiley & Sons, New York, 1975

[11] D J Grisser, S Glowinkowski, M D Ediger, Macromolecules, **24**, 4270 (1991)

STUDIA UNIV BABEŞ-BOLYAI, PHYSICA, XL, 1, 1995

NMR OBSERVATION OF THE SPIN-LATTICE RELAXATION OF PROTONS IN MOLTEN AND CROSS-LINK POLYBUTADIENE

M. TODICĂ[1], J.P. COHEN-ADDAD[2], A.V. POP[1] and G. DAMIAN[1]

ABSTRACT. - The spin lattice relaxation time of the protons was measured in molten and cross-link polybutadiene in order to obtain informations about the local dynamics of the polymeric chain We observed that, the curves describing the temperature dependence of the relaxation time are similarly for both polymers, over a large range of temperature above the glass-transition temperature, T_g A weak concentration of cross-link agent do not affect the local dynamics of polymeric chain.

INTRODUCTION

Spin-lattice relaxation rate depends on the strength of the dipolar interaction between the protons of the segmental unit, which include a few neighboring monomers This interaction is affected by the local dynamics of the polymeric chain Thus the relaxation time can provide informations about the local motion of the polymeric chain [1]

The existence of the topological constraints, as the entanglements or cross-link junctions between different polymeric chain, induces an effect of restriction of conformational fluctuations of chain skeletons More precisely, skeletal bonds are submitted to an average orientation order which exists along any chain segment embedded in a temporary network This orientational order is enhanced by the formation of cross-links [2] It is clear that the topological constraints, especially the cross-link junctions, affects the large amplitude motions of the polymeric chain, but is interesting to observe the effect of this constraints on the local dynamics [3]

EXPERIMENTAL

NMR measurements were made on the molten polybutadiene and the cross-link polymer obtained from this polybutadiene, in the temperature range from 234K to 350K The

[1] *"Babeş-Bolyai" University, Faculty of Physics, 3400 Cluj-Napoca, Romania*

[2] *Laboratoire de Spectrometrie Physique, "RMN-Polymers", 38402 Grenoble, France*

microstructure of the polybutadiene was defined by the following contents of monomeric units PB1 8% in the vinyl-1,2 conformation, 51% in the trans-1,4 conformation, and 41% in the cis-1,4 conformation The molecular weight of the polybutadiene was M_n = 70 000 g/mole and the glass-transition temperature was T_g=175±2 K The cross-link polymer, PBS, was obtained from this polybutadiene, using the sulfur as a cross-linking agent The concentration of the cross-linking agent was γ_c^s=0 01 g/mole We utilized also in ours measurements another polybutadiene, PB2, with a different microstructure and molecular weight respectively· 40% in the vinyl-1,2 conformation, 36% in the trans-1,4 conformation, 24% in the cis-1,4 conformation, M_n=190 000g/mole, and T_g=202±4 K All the samples were supplied and characterized by the Manufacture Michelin (France)

The samples were enclosed in NMR tubes and sealed under a primary vacuum Spin-lattice relaxation T_1 of the protons were measured using an inversion-recovery sequence (π-τ-π/2) [4] The values of the relaxation time were obtained by fitting the experimental data with a single exponential function

All the measurements were performed at 45 MHz, using a CXP Bruker spectrometer

RESULTS AND DISCUSSION

Spin-lattice relaxation is sensitive to the local dynamics of segmental chain An orientational order is induced in the molten polymer by the entanglements. Polymeric chain is divided in many segments including many monomeric units [5] Thus, the local mobility of segments is affected by this orientational order Dipolar interaction between the protons may be not averaged to zero, and thus the spin-lattice relaxation is characterized by a certain value of T_1

An supplementary order and then an supplementary division of the polymeric chains is induced in the cross-link polymers by the cross-link junctions We can assume that the segmental units of the polymeric chain were determined by the entanglements and the cross-link junctions This news segmental units may be different from those of the molten polymer if the concentration of the cross-link junctions is higher In this case we attempt that the spin-lattice relaxation rate be different for the molten and cross-link polymers When the concentration of the cross-link junctions is small the segmental unit is principally determined

by the entanglements, and then the spin-lattice relaxation rates for both polymers must be equals

We attempt that spin-lattice relaxation rates of the protons located in different sides of the monomeric unit have different values because theirs bond length are different Recent works, performed on polybutadiene samples shows that all the protons can be characterized by a single relaxation time T_1, and the local monomeric reorientations by a single correlation time τ_c,[6] Both T_1 and τ_c are temperature dependent The correlation time τ_c is simply related to the Larmor frequency ω_0 when the spin-lattice relaxation rate reach its maximum value In this case $\omega_0 * \tau_c = 1$, which means that the frequency of the local reorientation is equal to the Larmor frequency [7]

The temperature dependence of the relaxation time T_1 for molten and the cross-link polymers are shown in Fig 1

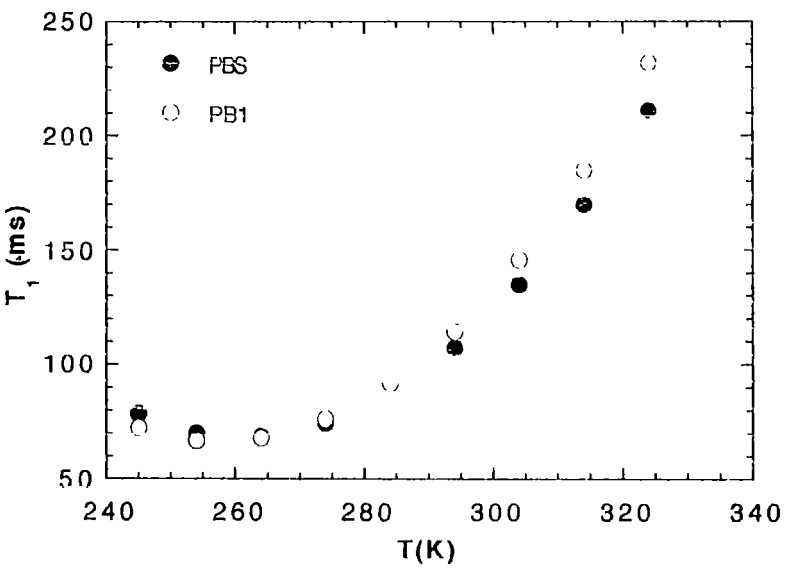

Fig.1. The temperature dependence of spin-lattice relaxation time of the molten polymer PB1 and the cross-link polymer PBS

We observed that the temperature dependence of T_1 is practically the same for both the polymers The minimum value of T_1 is T_{1min}=68±5 ms corresponding to θ=258±5K for both polymers We observed that $\theta=T_g+83\pm7$ K The calculated correlation time τ_c corresponding to this temperature is $\tau_c=2\ 2\ 10^{-8}$ s In the superposition temperature range of

$T_1(T)$, we can assume that the spin-lattice relaxation mechanism is the same for both polymers The local dynamics is not affected by the cross-link junctions A small concentration of the cross-linking agent do not affect the initial segmental unit of the molten polymer The correlation length of the local reorientations is smaller that the length between the cross-link junctions

A small difference of the absolute values of T_1 was observed in the high temperature domain The mobility of the entire polymeric chain is higher in the molten polymer that in the cross-link polymer This mobility affect the local dynamics and thus the relaxation rate In the cross-link polymer, the mobility of the entire chain is diminished by the cross-link junctions As a result the local dynamics and the relaxation mechanism are perturbed The changes of the molecular weight do not affect the local dynamics, but is interesting to observe the relaxation processes for the polymeric chains with a different microstructure

We performed measurements of the spin-lattice relaxation time in the PB2 sample which is a molten polymer with a different molecular weight and another microstructure than PB1 The temperature dependence of the spin-lattice relaxation time is shown in Fig 2

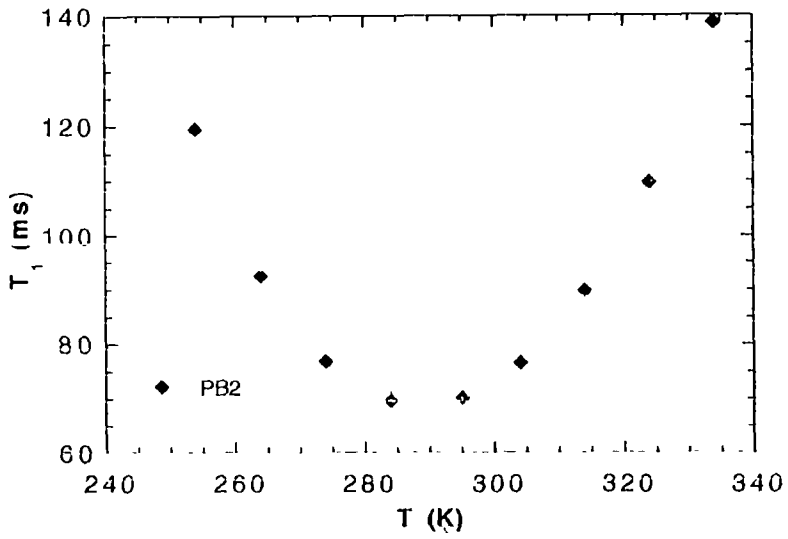

Fig.2. The temperature dependence of the spin-lattice relaxation time of the PB2 sample

The minimum value of the relaxation time is T_{1min}=68±5 ms, corresponding to the θ= 290 K For this temperature the correlation time of the local reorientation is τ_c=2 2 10^{-8}s The temperature is related to the glass-transition temperature by the relation· θ=T_g+88±5 K This relation suggest a new representation of the relaxation time T_1 versus a variable T-T_g In this representation the curves T_1(T-T_g) for all the samples are superposed (Fig 3)

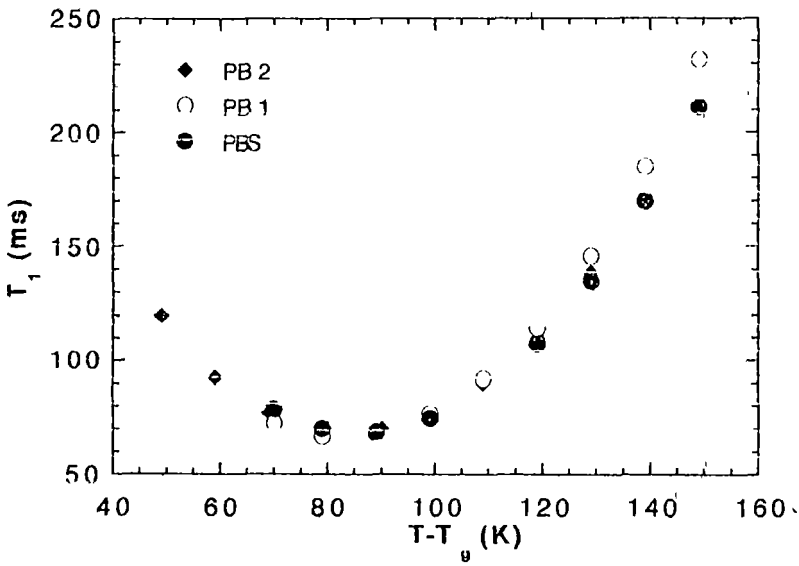

Fig.3. The superposition property of the spin-lattice relaxation time for the PB1, PbS and PB2 samples

The dependence of the relaxation time T_1 versus the T-T_g variable is the same The superposition property was observed in previous works performed in polyisoprene-toluene solutions [8] We can assume that the relaxation mechanism is not modified by changing the microstructure of the molten polymer Thus the segmental units and the local dynamics of the polymeric chain is not essentially affect by the change of the microstructure

CONCLUSION

The dominant mechanism which govern the nuclear relaxation of the protons of the polymeric chain is the dipolar interaction between the nuclear spins located within one given chain The spin-lattice relaxation mechanism is not significantly different in the molten and cross-link polymers A weak concentration of the cross-linking agent do not modify

essentially the local dynamics of segmental units

A superposition property of the relaxation time $T_1(T-T_g)$ was observed for polybutadienes with different microstructures The change in the microstructure of the polymeric chain do not affect the local mobility of the segmental units The minimum value of T_1 was observed at $\theta=T_g+85\pm8$ K for this samples The correlation time τ_c of the local reorientational motion, corresponding to this temperature, is $\tau_c=2\,2*10^{-8}$ s

REFERENCES

1 J P Cohen-Addad,"NMR and Fractal Properties of Polymeric Liquids and Gels", Pergamon Press, London, 1992

2 J P Cohen-Addad, E Soyez, A Viallat and J P Queslel, Macromolecules, 25, 1259 (1992)

3 P G De Gennes, "Scaling Concepts in Polymers Physics", Cornell University Press, Ithaca, New York, 1979

4 A Abragam, "Principles of Nuclear Magnetism", Oxford University Press, London, 1961

5 J Ferry, "Viscoelastic Properties of Polymers", 3rd ed , J Wiley Ed , New York, 1980

6 A Guillermo, R Dupeyre, and J P Cohen-Addad, Macromolecules, 23,1291(1990)

7 I Ya Slonim, A N Lynbimov, "The NMR of Polymers", Plenum Press, New York, 1970

8 M Todica, G Damian, D Ciurchea and A V Pop, Studia UBB, Physica XXXX,1,1995 (in press)

STUDIA UNIV BABEŞ-BOLYAI, PHYSICA, XL, 1, 1995

IR, EPR AND MÖSSBAUER INVESTIGATION OF SOME FE(III) COMPLEXES WITH ANTIINFLAMMATORY DRUGS

L. DAVID[1], O. COZAR[1], I. BRATU[2], V. CHIŞ[1] and Gh. BORA[3]

ABSTRACT. - Iron(III) complexes with antiinflammatory drugs Fe(aspirinate)$_3$ $2H_2O$, Fe(indomethacin)$_3$ $2H_2O$ and Fe(piroxicam)$_3$ 2DMF were prepared and investigated by IR, EPR and Mössbauer spectroscopies The complexes appear to have an octahedral stereochemistry involving three non-steroidal ligand molecules in the process coordination Powder EPR spectra of these complexes are characteristic to the dimeric species with the metallic ion in the high spin state (S=5/2) The Mössbauer parameters are typical for the covalent iron complexes

Introduction Many antiinflammatory agents have been developed to inhibit some component of the inflammatory process without correcting the cause of the disease or promoting tissue repair [1] These drugs may cause adverse reactions such as peptic ulceration and gastrointestinal bleeding [2]

The interest in the therapeutic use of the metallic compounds in treating connective tissue diseases has been significantly increased in the last years [3] Copper complexes of a number of non-steroidal antiinflammatory drugs have been shown to be more potent antiinflammatory agent and less ulcerogenic than the parent drugs [4] The present paper is a part of a study aimed to characterize the coordination compounds formed between non-steroidal antiinflammatory drugs and transition metal ions [5,6]

We present here the results obtained by IR, EPR and Mossbauer investigation on the complexes formed by iron(III) with some antiinflammatory drugs such as aspirinate, indomethacin and piroxicam The molecular structure of the ligands are shown in Fig 1

Experimental. The metal complexes were prepared by following procedure *Fe(III)(aspirinate)$_3$ $2H_2O$ and Fe(III)(indomethacin)$_3$ $2H_2O$* an amount of 0 11mols of

[1] *"Babeş-Bolyai" University, Faculty of Physics, 3400 Cluj-Napoca, Romania*

[2] *Institute of Isotopic and Molecular Technology, 3400 Cluj-Napoca, Romania*

[3] *Chemical Pharmaceutical Research Institute, 3400 Cluj-Napoca, Romania*

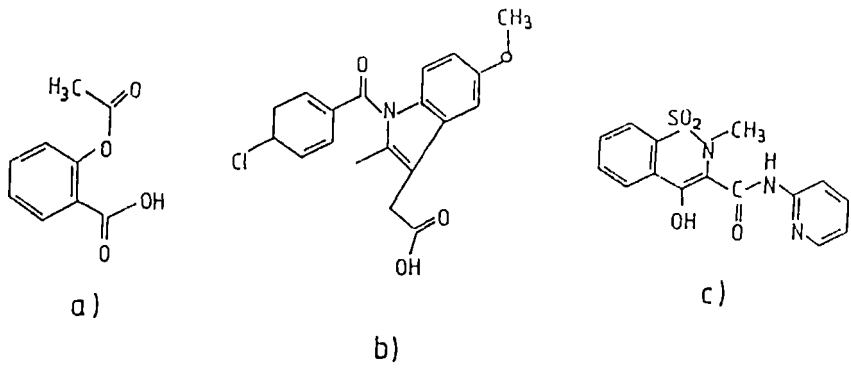

Fig.1. Molecular structures of aspirinate (a), indomethacin (b) and piroxicam (c)

antiinflammatory drug (aspirinate and indomethacin respectively) was dissolved in 50ml of ethanol and 0 2 mols of $FeCl_3$ were also dissolved in 100 ml of water These two solutions were mixed and stirred for about 1 hour and then an amount of 200ml water was added to the above solution The precipitate was filtered and washed with water Finally it was dried in air at room temperature

Fe(III)(piroxicam)$_3$ 2DMF 0 11 mols of piroxicam were dissolved in 100 ml of dimethylformamide (DMF) A $FeCl_3$ solution, prepared by adding 0 05mols of $FeCl_3$ to 100ml of ethanol-water mixture (1 1) was added to the first solution This mixture was refluxed under stirring for about 0 5hour at 60°C The precipitate was filtered, washed with methanol and then dried in air at room temperature

IR absorption spectra in the 400-3600cm^{-1} range were recorded with an IFS 48 Bruker spectrometer using the KBr pellets technique

EPR spectra were recorded at 9 4GHz using a standard JEOL-JES 3B spectrometer

The Mossbauer spectra were obtained with an ELRON spectrometer using a ^{57}Co/Pd source The calibration of the spectrometer was carried out at constant acceleration assuming a Lorentzian shape of the lines with computer code using the Gauss-Newton algorithm with the Levenberg-Marquart option

Results and discussion Characteristic IR spectra of the Fe(III)(aspirinate)$_3$ 2H$_2$O compound are shown in Fig 2 The band observed at 1700cm^{-1} and 1765cm^{-1} is assigned to

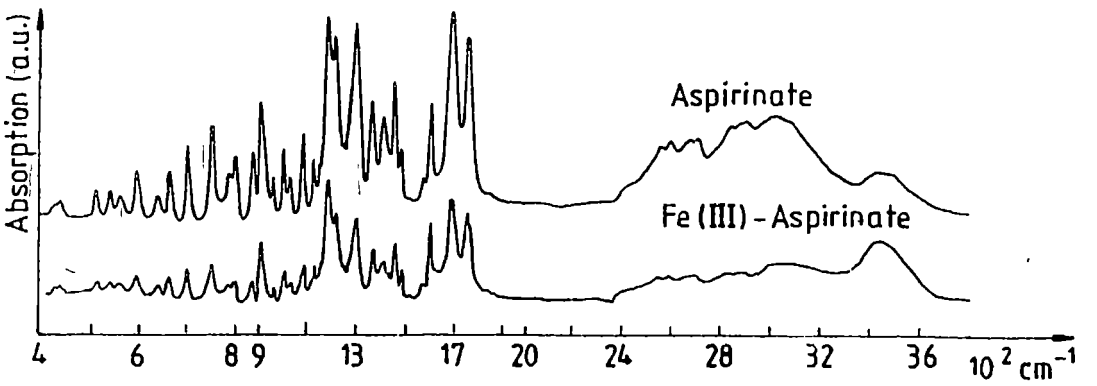

Fig.2. IR spectra of aspirinate and Fe(III)-aspirinate complex

the stretching vibration of the carbonyl group of aspirin Both bands are strongly diminished in intensity in the complex spectrum and are shifted at 1690cm^{-1} and 1755cm^{-1} respectively This fact indicates the involving of the carbonyl group in the metal ion coordination

In Fe(III)-aspirinate complex the antisymmetric carboxylate stretching vibration is shifted from 1615cm^{-1} to 1605cm^{-1} while the symmetric stretching vibration is lowered from 1315cm^{-1} to 1305cm^{-1} indicating the involving of this group at coordination

The band centred at 3440cm^{-1} in the remaining hydrated complex suggest the presence of hydrogen bonded water molecules

The band observed at 435cm^{-1} may be attributed to the Fe-O stretching vibration

Fig 3 shows the IR spectra of Fe(III)(indomethacin)$_3$ $2H_2O$ complex The band observed at 1700cm^{-1} and 1720cm^{-1} in the free ligand are assigned to the carbonyl group. These bands appear in the spectrum of the metal complex at 1690cm^{-1} and 1710cm^{-1} respectively The carboxylate stretching vibration is also shifted from 1620cm^{-1} to 1605cm^{-1}

The absorption band from 3450cm^{-1} is due to the O-H stretching vibration of the ligand water molecules

IR spectrum of the piroxicam (Fig 4) shows an absorption band centred at 3350cm^{-1} characteristic to an O-H stretching vibration The drug is reacted as the enolate anion such as no O-H vibration is expected in the complex [7]

The band observed at 1630cm^{-1} in the free ligand is assigned to the carbonyl stretching vibration of the secondary amide group -CO-NH, and it is lowered by 10cm^{-1} in the IR

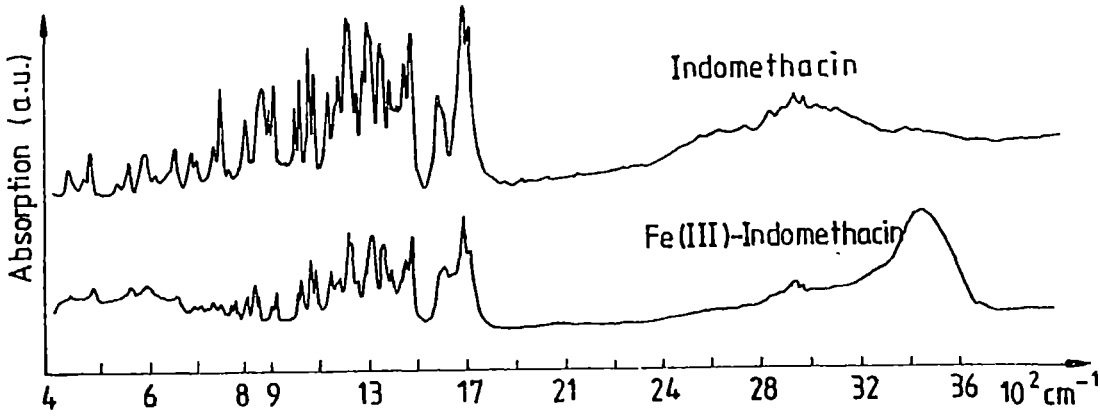

Fig.3 IR spectra of indomethacin and Fe(III)-indomethacin complex

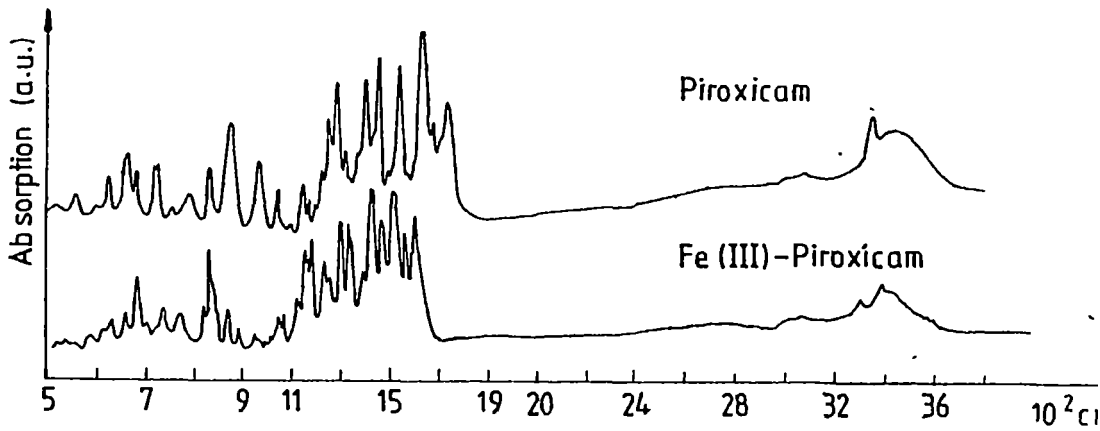

Fig.4. IR spectra of piroxicam and Fe(III)-piroxicam complex

spectrum of the complex

X-ray diffraction studies of some piroxicam metal complexes have indicated that metal ion is six-coordinated though carbonyl oxygen atoms of the secondary amide group and the pyridil nitrogen atom of the ligand molecules The axial positions along the oz axis are occupied by two DMF molecules bonded to the metal through their carbonyl oxygen atoms [8]

At 1310cm^{-1} and 1170cm^{-1} the IR spectra presents two strong bands which are typical for_vas(SO2) and_vs(SO2) vibrations The bands corresponding to the deformation vibration of the SO2 group appear at 530cm^{-1}

EPR spectra of these complexes suggest that the iron(III) ion is in the high-spin form (S=5/2) in the ground state, all the spectra being almost isotropic (g=2 002) [9]

The shape of the EPR spectra suggests the presence of the dimeric species analogous to those observed in the case of the copper(II) complexes with the same ligands [5,6] The coupling of metal ions is realized by a strong exchange interactions

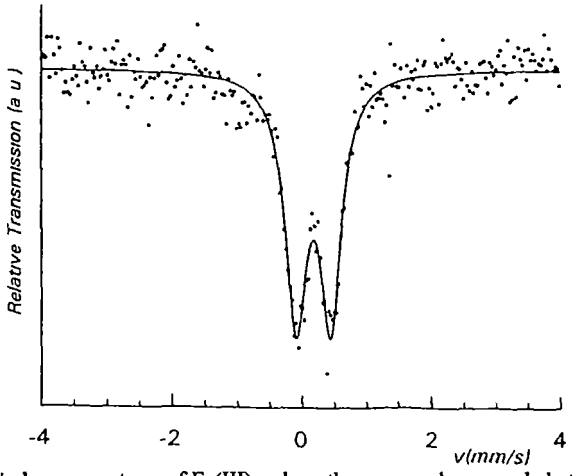

Fig.5 Experimental Mössbauer spectrum of Fe(III)-indomethacin complex recorded at room temperature The solid line shows the simulated spectrum with the parameters given in Table 1

The high spin ferric states of the iron ions are clearly established by ^{57}Fe Mossbauer data All tree iron-antiinflammatory complexes studied in this work are characterized by a single quadrupolare-split doublets (Fig 5), with isomer shifts ranging from +0 40 to +0 57mm/s (Table 1) These isomer shifts values are well within the range expected for trivalent iron and the quadrupole-splitting parameters substantiate the high spin nature of each ferric ion [10]

Table 1. The Mössbauer parameters for some Fe(III)-antiinflammatory drugs complexes

Complex	δ (mm/s)	ΔEQ (mm/s)
Fe(aspirinate)$_3$ $2H_2O$	0 40	0 68
Fe(indomethacin)$_3$ $2H_2O$	0 55	0 70
Fe(piroxicam)$_3$ 2DMF	0 57	0 71

Conclusions The IR spectra of the Fe(III)-antiinflammatory drugs aspirinate, indomethacin and piroxicam shows that in these complexes the iron(III) ion is in a pseudo-octahedral environment being coordinated by three ligands molecules EPR spectra of these complexes shows that the metallic ion is in the high spin state (S=5/2) with a pseudo-octahedral local symmetry and strongly coupled by exchange interactions This fact is confirmed also by Mössbauer spectroscopy

REFERENCES

1 J M McCord, Science, 185,529(1974)
2 B M Sutton, Annu Rep.Med.Chem., 14,321(1979)
3 J R J Sorenson, Metal Ions in Biological Systems, (H Sigel, Ed), Vol 14, Marcel Dekker, New York, 1982, p 77-124
4 D H Brown W E Smith J W Teape, A J Lewis, J Med.Chem , 1980, 23,729
5 L David, O Cozar, V.Chiş, A.Negoescu, I Vlaşin, Appl Mag.Reson , 6,521(1994)
6 O Cozar, L David, V Chiş, C Cosma, V Znamirovschi, G.Damian, I Bratu, Gh Bora, Appl Mag.Reson , 8,235(1995)
7 A Bury, A E Underhill, D R Kemp, N J O'Shea, J P Smith, P.S.Gomm, Inorg Chim Acta, 1987, 138,85
8 R Cini, G Georgi, A Cinquantini, C Rossi, M Sabat, Inorg Chem., 29,5197(1990)
9 A Bencini, D Gatteschi, Trans.Met Chem , 1982, 8, 1
10 S L Kessel, R M Emberson, P G.Debrunner, D N Hendrickson, Inorg Chem , 19,1170(1980)

STUDIA UNIV BABEŞ-BOLYAI, PHYSICA, XL, 1, 1995

TRANSPORT PROPERTIES OF THE $YBa_2(Cu_{1-x}Fe_x)_3O_y$ SUPERCONDUCTOR

Gh. ILONCA[1], A.V. POP[1], A. LANCKBEEN[2], M. MEHBOD,[2] D. CIURCHEA[1], M. ILONCA[1] and R. DELTOUR[2]

ABSTRACT. - Bulk samples of the high T_c superconductor $YBa_2(Cu_{1-x}Fe_x)_3O_{7-\delta}$, with $0<x<0.08$ have been investigated by measurements of the Hall effect and of the electrical resistivity, in the temperature range 20 K - 300 K with magnetic fields up to 5 T The X - ray diffraction analysis shows an orthorhombic-pseudo-tetragonal phase transition at $x = 0.035$ The temperature dependence of the hole carrier concentration showed an anomaly around $T \approx 230K$

Introduction Chemical substitution of magnetic ions in $YBa_2Cu_3O_y$ (YBaCuO) offers an interesting approach for the investigation of the properties of the high T_c superconductors The substitution of magnetic rare-earth ions at the Y site produces little effect on T_c, despite the large magnetic moments of the substitution ions [1-2]

Cu substitution by Fe in YBaCuO produces several interesting effects on the structure and superconductivity,as it drives the system towards a tetragonal structure without severely depressing T_c [3,4-10] Mössbauer spectroscopy measurements, with the support of other techniques, X - ray absorption fine structure analysis [11] and magnetic susceptibility measurements [7] show a variation of the magnetic moment from $2.5\mu_B$ to $4.9\mu_B$ [12] The measured moment could be an average for the magnetic moment of Fe substituted in both Cu(1) and Cu(2) sites with different electronic configurations, as the theoretical value of the magnetic moment for a d^5 ion has two possible values $\mu = 2.2\mu_B$ for the low-spin quantum state and $\mu = 5.9\mu_B$ for the high-spin quantum state

The studies by electron diffraction and high resolution electron microscopy [13] have shown the existence of a finer "tweed" structure of overlapping lenticular domains oriented

---

[1] *"Babeş-Bolyai" University, Faculty of Physics, 3400 Cluj-Napoca, Romania*

[2] *Université Libre de Bruxelles, CP 233 Physique des Solides, B-1050 Bruxelles, Belgium*

along [<120>] and [<110>] and associated diffuse streaks also [14] These diffuse streaks have been attributed to microdomains of the orthorhombic phase containing small areas of the tetragonal phase associated with the Fe substituent This microdomain structure varies with the Fe concentration and the preparation method

Among the interesting properties observed in the cuprate superconductors, mention should be made on the normal-state transport properties and more particularly on the temperature dependence of the Hall coefficient, $R_H(T)$ In YBaCuO,approximate descriptions of the temperature dependence of the Hall number n_H and of the electrical resistivity, $\rho(T)$, are often given by the equations

$$n_H = \frac{1}{R_H \cdot e} = a \cdot T + b \qquad (a,b>0) \tag{1}$$

$$\rho(T) = \rho(0) + c \cdot T \qquad (c>0) \tag{2}$$

Since the Hall data on YBaCuO are rather sparse [4, 17, 25], Eq (1) has not been thoroughly tested For this reason in this work we have simultaneously measured $\rho(T)$ and $R_H(T)$ in bulk $YBa_2(Cu_{1-x}Fe_x)_3O_y$

Experiment and techniques. A series of $YBa_2(Cu_{1-x}Fe_x)_3O_y$ samples were prepared,starting from $BaCO_3$, Y_2O_3, CuO and Fe_2O_3 powders, mixed in polyethylene jars with ZrO_2 beads in H_2O for two hours The powder was dried and pressed at 300 bar to obtain pellets Calcination was carried out at 905°C for 160 hours under O_2 flow (heating rate 3°C /min and cooling rate 0 5°C /min) The pellets were then ground in SiO_2 jars with SiO_2 balls, the powders were sieved (Φ 25 μm), pressed into pellets and fired at 930°C under O_2 flow for 12 hours (heating rate 3°C /min and cooling rate 0 5°C /min) This process was repeated twice The pellets then were sintered at 950°C under O_2 flow (heating rate 3°C /min and cooling rate 0 5°C /min) for 12 hours and oxygenated at 500°C during 72 hours

Examination by X-ray diffraction (XRD), thermogravimetric analysis (TGA), energy

dispersion X-ray analysis (EDAX), scanning electron microscopy (SEM) and optical microscopy were performed The oxygen content in the sample was determined by the iodometric titration method Single phase material was obtained and the homogeneity of the Fe distribution in the grains was checked at the resolution level of the EDAX analysis

In order to perform precise Hall measurements, it was essential to minimize the misalignment of the Hall arms and also to achieve low contact resistances With this goal, a sample was cut from a pellet into a fine Hall-barr shape To obtain good electrical contacts, five pads were painted with silver-epoxy adhesive onto the Hall-bar shape and tempered at 400°C in air for 20 min Gold wires were finally attached with silver paste The contact resistance depended on the bulk resistivity of the sample, but was typically less than $2 \cdot 10^{-4}$ $\Omega \cdot cm^2$

We have measured the resistivity and the Hall voltage (ac-current) using a lock-in technique (Princeton Applied Research, Model 5210) in magnetic fields up to 5 T, in the temperature range 20 K - 300 K For dc-measurements, a Keithley 220 programmable current source, a Keithley 182 sensitive digital voltmeter and a Keithley 181 nanovoltmeter were used The current intensity passed through the sample was between 1 and 10 mA The standard procedure of taking data for both polarities of the current and the magnetic field, to cancel out thermal emf and resistivity components, was followed The temperature dependence of the resistivity in zero field was measured in the same run also in a separate run

Results and discussions. The patterns of the X-ray diffraction show that the samples are of single-phase material The lattice parameters a,b and c (shown as c/3) calculated from the diffiaction peak positions by a standard least squares refinement method, are shown in Fig 1 for x between 0 and 0 16 As x increases,the parameters a and b reach the same value for x = 0 035, indicating a nearly tetragonal symmetry beyond this range This value is in

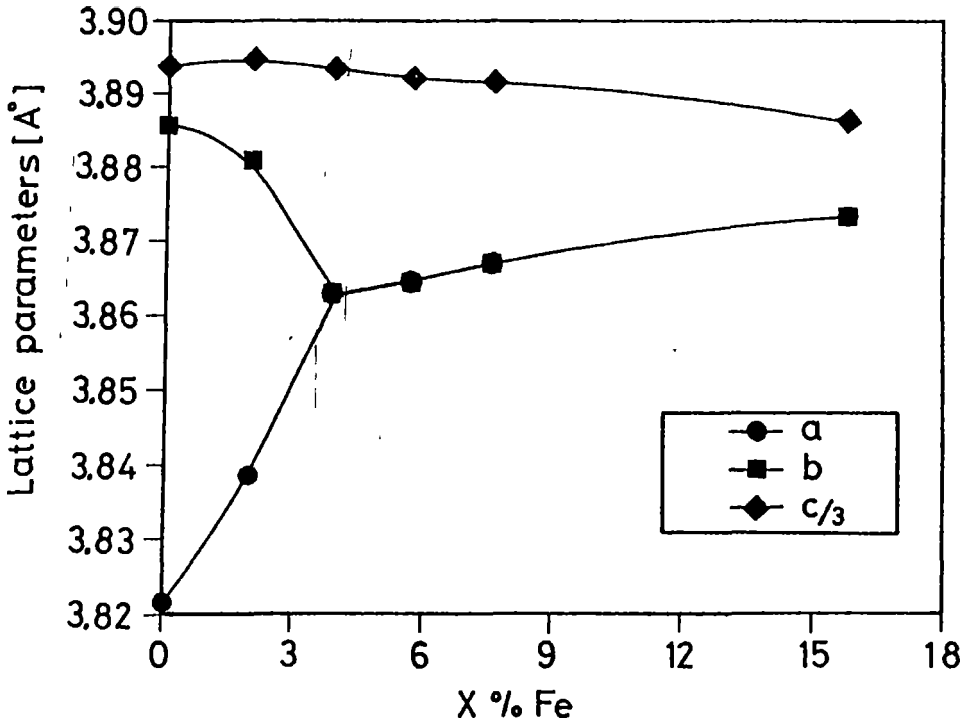

Fig.1. Lattice parameters a, b and c (presented as c/3) versus the Fe concentration. The lines are a guide for the eyes

agreement with results reported by other workers [10, 15-16]. The concentration at which the orthorhombic-tetragonal transition of this material appears,varies between x = 0 03 - 0 05 [17,18,19,20] depending on the synthesis procedure.

Figure 2 shows the temperature dependence of the electrical resistivity for $YBa_2(Cu_{1-x}Fe_x)_3O_y$ with x=0, y=6 96; x=0.02, y=6 95, x=0.039, y=7 00, x=0 058, y=7 02 and x=0.076, y=6.96 All the samples shows metallic behavior in the normal state With increasing dopant concentration, the resistivity curves are shifted upwards

The slope dρ/dT is altered by the impurity scattering as shown in Fig 3, where the residual resistivity versus the x-content, obtained by extrapolation of the resistivity curves at T = 0 K,is also plotted The slope increases with the impurity concentration from 0 025 (μΩ·cm/K) to 2 65 (μΩ·cm/K) and the residual resistivity from 0 025 (mΩ·cm) to 2

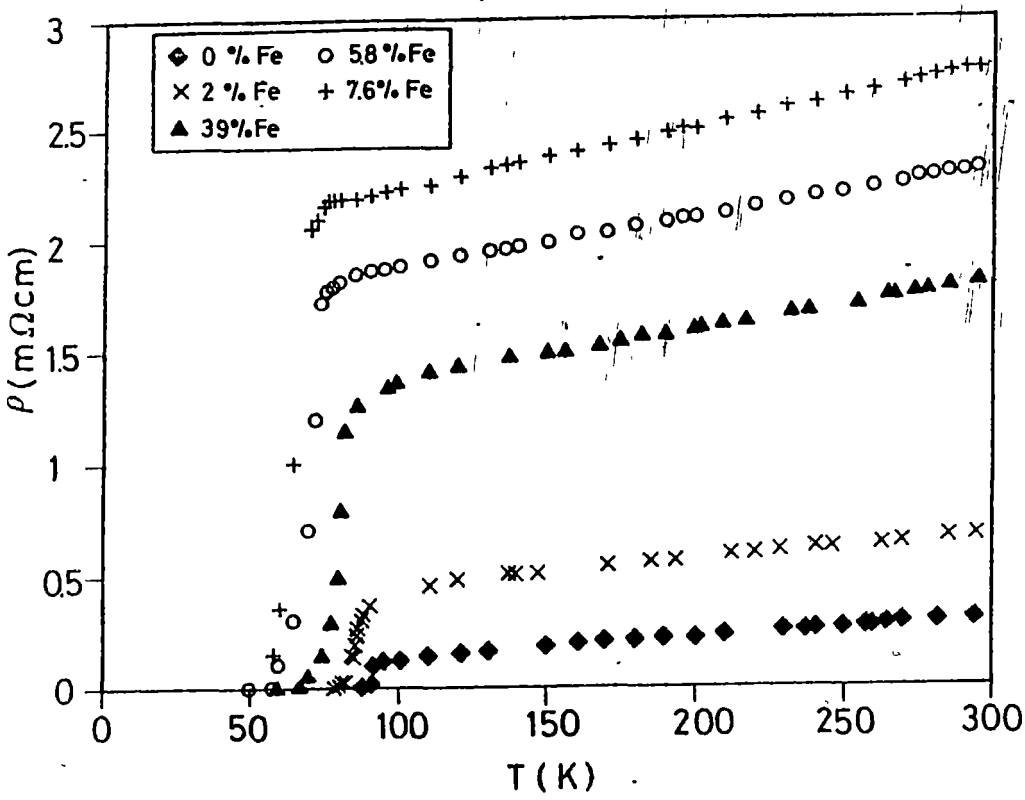

Fig.2. The temperature dependence of the electrical resistivity in the bulk $YBa_2(Cu_{1-x}Fe_x)_3O_y$

(mΩ·cm) It is known that a lack of oxygen increases the resrdual resistivity and the slope dρ/dT [21] but in our samples, the oxygen concentration is almost the same (y≈7) and so most of the observed effects can be attributed to the iron substitution at the Cu sites.

Between the substitution values x = 0.02 and x = 0 039 where the orthorhombic - tetragonal transition takes place, as illustrated clearly in Fig 1, we observe a change in the slope of the resistivity

T_c, defined as the midpoint of the superconducting transition temperature, with its corresponding width ΔT_c, calculated from the resistivity data,are plotted in the insert of Fig 3 The bars indicate the width of the transition defined by the 10 % and 90 % value of the resistivity transition It should be noted that the variation of T_c in the Fe substituted system

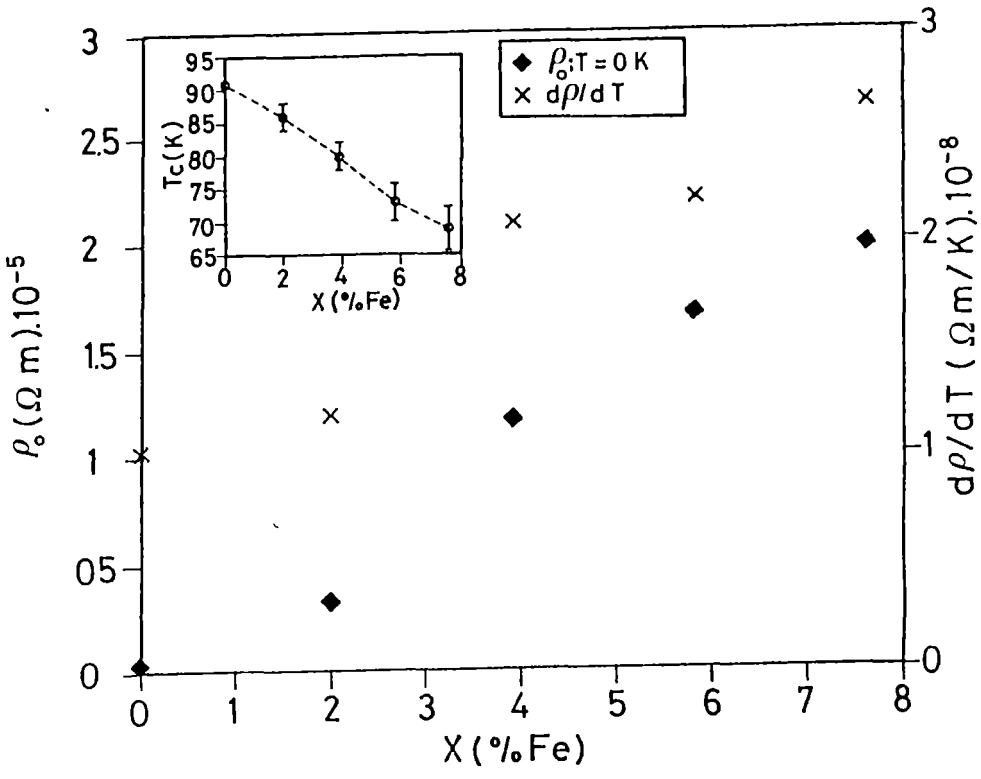

Fig.3. The variation of the residual resistivity ρ_0, the slope dρ/dT and the superconducting transitiontemperature T_c vs x [at %] in the bulk $YBa_2(Cu_{1-x}Fe_x)_3O_y$

is not completely linear with respect to the iron content, but we did not observe a constant value, as reported by others workers for the lower iron contents [6]

The temperature dependence of the Hall coefficient was measured We observed an increase in the Hall coefficient and a decrease in the transition temperature with increasing iron content There is a systematic upward shift of the curves with increasing iron concentration From the Hall constant R_H the Hall concentrations of charge carriers per unit cell were calculated, using the formula $n_H \cdot V = V_c / R_H \cdot e$, where V is the volume of the unit cell The temperature dependence of $n_H = 1 / R_H \cdot e$ for the Fe-doped samples is shown in Fig 4 At the various concentrations studied (x = 0 0 - 0 076),we found that the temperature

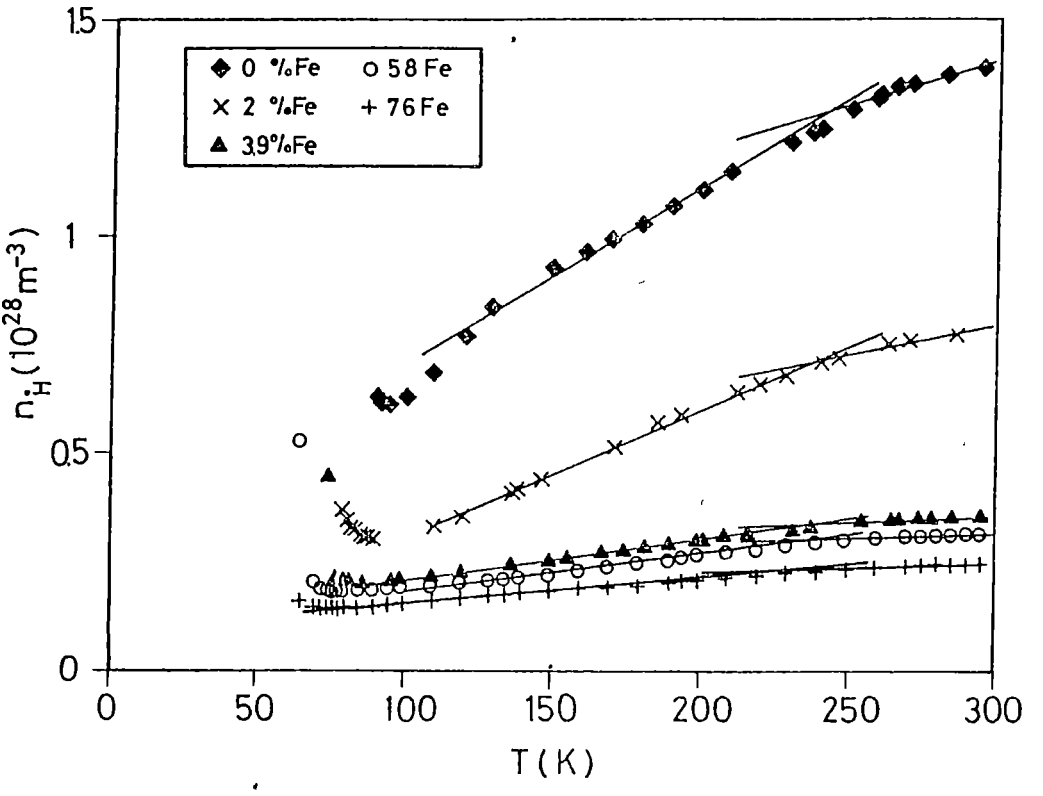

Fig.4. The temperature dependence of the Hall number n_H in the bulk $YBa_2(Cu_{1-x}Fe_x)_3O_y$ The line is a guide for the eyes

dependence of n_H does not follow a single straight line over the whole temperature range This is in partial agreement with theoretical results presented by Ioffe et al [22] and Nagaosa et al [23]. Deviations from the linear behavior above 230 K were evidenced The $n_H(T)$ dependence in the temperature range 125 - 230 K is described with a linear expression $n_H = \alpha \cdot T + \beta$ but also between 230 - 300 K

The slope $d(n_H \cdot V)/dT$, calculated from the data of Fig. 4, and the volume V of the unit cell decrease with x from 0 0076 hole V/K for x = 0 0 to 0 0047 hole V/K for x=0 02 with the samples in the orthorhombic structure and from 0 0015 hole V/K for x=0 0039 to 0 0008 hole V/K with the samples in the "tetragonal" structure We would like to point out the small variation in the hole concentration with temperature in the "tetragonal" structure,

in comparison with its large variation in the orthorhombic structure

The decrease in the "Hall slope", $d(n_H \cdot V)/dT$, with the increasing Fe impurities is correlated with the reduction of T_c A similar correlation was observed by Clayhold et al [24] with $YBa_2Cu_{3-x}M_xO_{7-\delta}$ (where M = Zn, Co),by Suzuki et al [25] with $La_{2-x}Sr_xCuO_4$ when the Sr content is altered and by Shimakaura et al [26] with $Tl_2Ba_2CaCu_2O_{8-\delta}$ when the oxygen content is varied

Mossbauer measurements [27] show that Fe substitutes for Cu in the chains and in the planes At low concentration, iron is located mainly in the chains and, by charge transfer, induces a drastic decrease in the hole carrier concentration A change in the iron distribution at higher concentrations ($x > 0\ 035$) could be at the origin of the change in $n_H \cdot V$, T_c and $d\rho/dT$, in addition to the influence of a Fe induced pair breaking mechanism [9].

In our 123 Fe doped system the deviations from the linear $n_H(T)$ dependence are similar to the slope change obtained in $YBa_2(Cu_{1-x}Zn_x)_3O_{7-\delta}$ [28], $Y_{1-x}Gd_xBa_2Cu_3O_{7-\delta}$ [29] and $(Bi_{1\,6}Pb_{0\,4})(Sr_{1\,8}Ba_{0\,2})Ca_2(Cu_{1-x}Cr_x)_3O_y$ [30] More recently, the temperature dependence of specific heat, the slope of lattice parameter c and the Mössbauer parameters for ^{57}Fe doped $YBa_2Cu_3O_{7-\delta}$ reveal anomalies near 230 K [31] This indicates that there exists a mobile boundary between two "phases" with slightly different lattice constants [31]

Conclusions We report an investigation of Fe substitution effects in bulk $YBa_2(Cu_{1-x}Fe_x)_3O_y$, prepared by a standard solid-state reaction X-ray diffraction analysis shows an orthorhombic - pseudo-tetragonal transition around $x = 0\ 035$, affecting also the resistivity and the Hall data

The linear temperature dependence of the resistivity was observed for all the doped samples from 100 - 300 K The temperature dependence of the carrier concentration show two anomalies around Tc and at T = 230 - 240 K With decreasing temperature starting from 300 K, the carrier concentration linearly decreases down to $T \approx 230$ - 240 K , at this temperature,

the slope changes and the carrier concentration continues to linearly decrease to a minimum value at a temperature T close to T_c These variations in YBaCuO doped with iron may be caused by a subtle change in the "ionic lattice" rather than in the electronic structure

Acknowledgement This work was supported by the Belgian SPPS Superconductivity SUPRANAT Contract SU 002/009

REFERENCES

[1] D W Murphy, S Sunshine, R B VanDover, R.J. Cava, B. Batlogg, S M Zahurak and L F Schnemeyer, Phys Rev. Lett **58**,1888 (1987)

[2] J M Tarascon, W R McKinnon, L H Greene, G W Hull and E M Vogel, Phys Rev **B36**, 226, (1987)

[3] J M Tarascon, P Barboux, P E Miceli, L H Green, G W Hull, M Eibschulz and S A Sunshine, Phys Rev **B37**, 7458, (1988).

[4] T R Chien, Z Z Wang and N P Ong, Phys Rev.Lett , **67**, 15, 2088, (1991)

[5] J Xu, M Suenaga, J Tafto, R L Sabatini, A R Moodenbaugh and P. Zolleker, Phys Rev , **B39**, 6667 (1989)

[6] K Westorholt, H J Wuller, H Bach, and P Stauche, Phys Rev , **B39**, 11680 (1989)

[7] L Nunez and R D Rogers, Phys Rev , **B44**, 4526 (1991)

[8] A Matsushita, H Aoki and T Matsumoto, Physyca **C166**, 100, (1990)

[9] M Mehbod and P Wyder, R Deltour, Ph Duvigneaud and G Naessens, Phys Rev., **B36**, 8819 (1987)

[10] B D Dunlap, J D Jorgensen, W K Kwon, C W Kimball, J L Matykiewicz and H Lee, Physica,**C153-155**, 1100 (1988)

[11] A Koizami, H Maeda, N Bamba, H Maniyama, E Takayama Muromachi, J Shi, K Shimizi, M Mino and H Yakamazi, Jpn J Phys ,**28**, L 203 (1989)

[12] A Junod, A Bezinga, D. Eckert, T Graf and J Muller, Physica, **C152**, 485, (1988)

[13] T Krekels, G Van Tendeloo, D Broddin, S. Amelinckx, L Tanner, M Mehbod, E Vanlathem and R Deltour, Physica **C173**,361 (1991)

[14] P Bordet, J H Hodeau, P Strobel, M Marezio and A Santoro, Solid State Commun , 66,435, (1988)

[15] H B Tang, Y Ren, Y L Liu, Q W. Yan and Z Zhang, Phys Rev , **B39**, 12290, (1989)

[16] M Ishikawa, T. Takabatake, A Tohdake, Y Nadazawa, T Shibuya and K Koga, Physica, **C153-155**, 890 (1988)

[17] R Suryanarayana, G T Bhandage, M. Rateau, O. Gorochox, H Pankowska, M Ghorayev, G Villers and C Vard, Journal Less Comm Metals, **151**, 109 (1989)

[18] T Tamaki, T Komai, A Ito, Y Maeno and T Fujita, Solid State Comm , **65**, 43, (1988)

[19] V A Trounov, T Yu, Kaganovich, A J Kurbakov, A V Matveev, A M Balagurov, A W Hewat, P Fischer, O Antson and R M A. Maayouf, Physica C **197**,123 (1992)

[20] S Katsuyama, Y Ueda and K Kosuge, Physica **C165**, 404, (1990)
[21] J R Cooper, D D Oberteli, A Carrington and J W Loram, Phys Rev , **B44**, 12086, (1991)
[22] L B Ioffe and P B Wiegmann, Phys Rev , **B43**, 1219 (1991)
[23] N Nagaosa and P Lee, Phys Rev **B43**, 1233 (1991)
[24] J Clayhold, N P Ong, Z Wang, J M Tarascon and P Barboux, Phys Rev , **B39**, 7324,(1989)
[25] M Suzuki, Phys Rev ,**B39**, 2312, (1991)
[26] Y Shimakawa, Y Kubo, T Manako and H Igarashi, Phys Rev, **B40**, 11400, (1989)
[27] M G Smith, R D Taylor and H Oesterreicher, Phys Rev , **B42**, 4202, (1990)
[28] Gh. Ilonca, M Mehbod, A Lanckbeen and R Deltour, Phys Rev , **B47**, 15265, (1993)
[29] A V Pop, D Ciurchea, V Pop, I Cosma, Gh. Ilonca, Supercond Sci and Technol , 7, 558, (1994)
[30] A V Pop, Gh Ilonca, D Ciurchea, V Pop, L A Konopko, I I Geru, M Todică, V Ioncu, Int J Mod Phys **B9**, 695 (1995)
[31] V M Cherepanov, M A Chuev, E Tsymbal, Ch Sauer, W Zinn, S A Ivanov, V V Zhurov, Solid State Commun., **93**, 921, (1995)
[32] Y Iye, Physical Properties of High-Temperature Superconductors III, Ed by D M Ginsberg, World Scientific Singapore, New Jersey, London, pg 287 (1992)

STUDIA UNIV BABEŞ-BOLYAI, PHYSICA, XL, 1, 1995

ON THE MAGNETIC BEHAVIOUR OF $(Y_{1-X}Zr_X)M_3$ COMPOUNDS WHERE M = Co OR Fe

E. BURZO[1] and R. TETEAN[1]

ABSTRACT. - The magnetic properties of $(Y_{1-X}Zr_X)M_3$ compounds with M = Co or Fe were investigated in the temperature range 5-900 K and fields up to 70 kOe The compounds are ferromagnetically ordered The mean iron moments are little dependent on composition while cobalt shows a weak ferromagnetism. Above the Curie temperatures the reciprocal susceptibilities follow a Curie-Weiss behaviour Finally the magnetic behaviour of the above compounds is analyzed in correlation with crystal structure

1. Introduction. The YM_3 compounds with M=Co or Fe crystallize in $PuNi_3$-type structure having R $\bar{3}$ space group In this structure there are two non-equivalent yttrium sites and three non-equivalent M sites [1,2] $ZrCo_3$ shows a $MgCu_2$ -, type structure [3] The $(Y_{1-X}Zr_X)Co_3$ system crystallizes in a $PuNi_3$ - type structure in the composition range $x<07$ This changes to four slabs hexagonal structure for $0\,7<x<0\,9$ and then to $MgCu_2$ - type structure for x=1 0 [4]

The YM_3 compounds are ferromagnetically ordered [2,5,6] The magnetic moments of cobalt and iron are dependent on the lattice sites[2] By magnetic measurements only their mean values may be obtained

Previously we reported some preliminary results concerning the magnetic properties of $(Y_{1-X}Zr_X)Co_3$ system [7]. As an one going work on the magnetic properties of pseudobinary compounds we studied comparatively the magnetic properties of the Fe and Co in $(Y_{1-X}Zr_X)M_3$ compounds Different magnetic behaviour is evidenced for the above 3d transition metals

2. Experimental. The compounds were prepared by arc melting the constituents on a water - cooled cooper hearth under purified argon atmosphere The samples were thermally

[1] *"Babeş-Bolyai" University, Faculty of Physics, 3400 Cluj-Napoca, Romania*

treated in vacuum for one week at temperature which dependend on the composition The X-ray analysis of $(Y_{1-X}Zr_X)M_3$ confirms the previous reported compositional sequence of structure Magnetic measurements were performed in the temperature range 5 - 900 K and external fields up to 70 KOe The spontaneous magnetization, M_s were determined from magnetization isotherms, according to approach to saturation law Above the Curie temperatures the magnetic susceptibilities were obtained by using a Faraday - type balance

3. Experimental results The thermal variations of spontaneous magnetizations for $(Y_{1-X}Zr_X)M_3$ compounds are shown in Fig 1 (M=Co) and Fig 2 (M=Fe) The magnetic data suggest a ferromagnetic type ordering

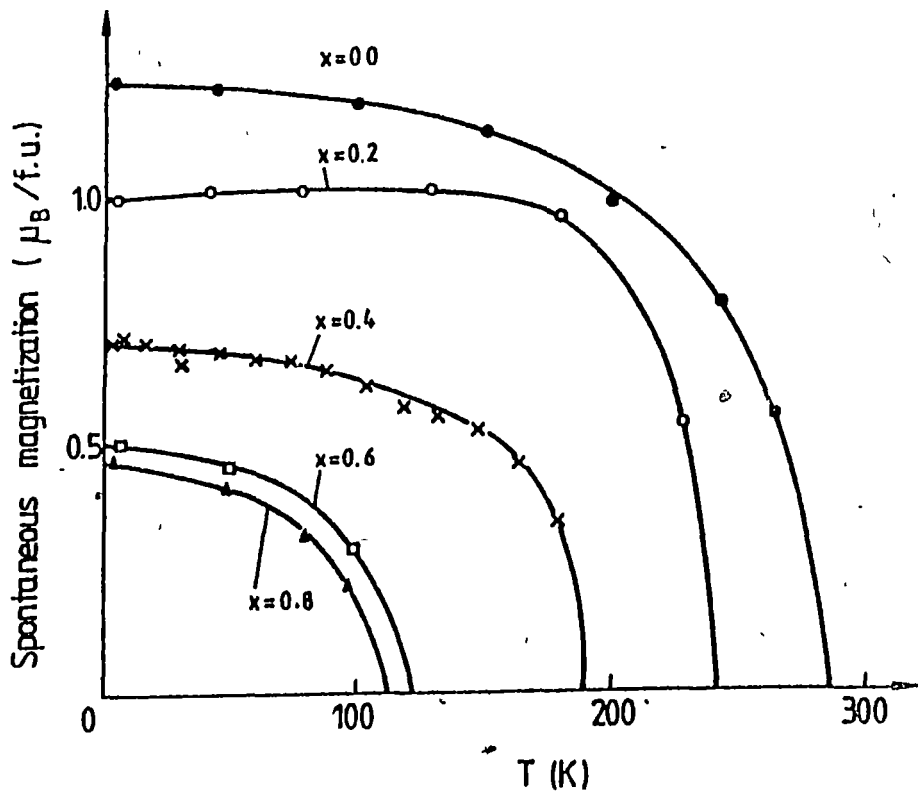

Fig.1. Temperature dependences of the spontaneous magnetizations of $(Y_{1-X}Zr_X)Co_3$ compounds

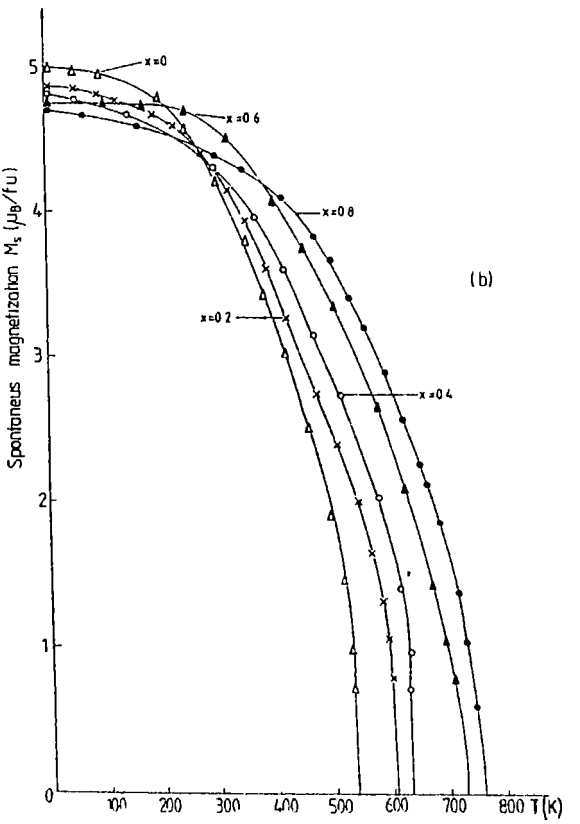

Fig.2. Temperature dependences of the spontaneous magnetizations of $(Y_{1-x}Zr_x)Fe_3$ compounds

The composition dependence of the spontaneous magnetisations, M_s, at 5 K and of the Curie temperatures, T_c, are shown in Fig 3 For M = Co both M_s and T_c values decrease when increasing zirconium content The spontaneous magnetization of iron compound decrease only little, while the Curie temperatures increase when increasing zirconium content

Above the Curie temperatures, the reciprocal susceptibility obey linear temperature dependences - Fig 4 The effective M moments determined from Curie constants are plotted in Fig 3 The effective iron moments are nearly constants while the cobalt effective moments increase as the zirconium content is higher

The experimental data show that the magnetic behaviour of cobalt and iron, in similar compounds, is different

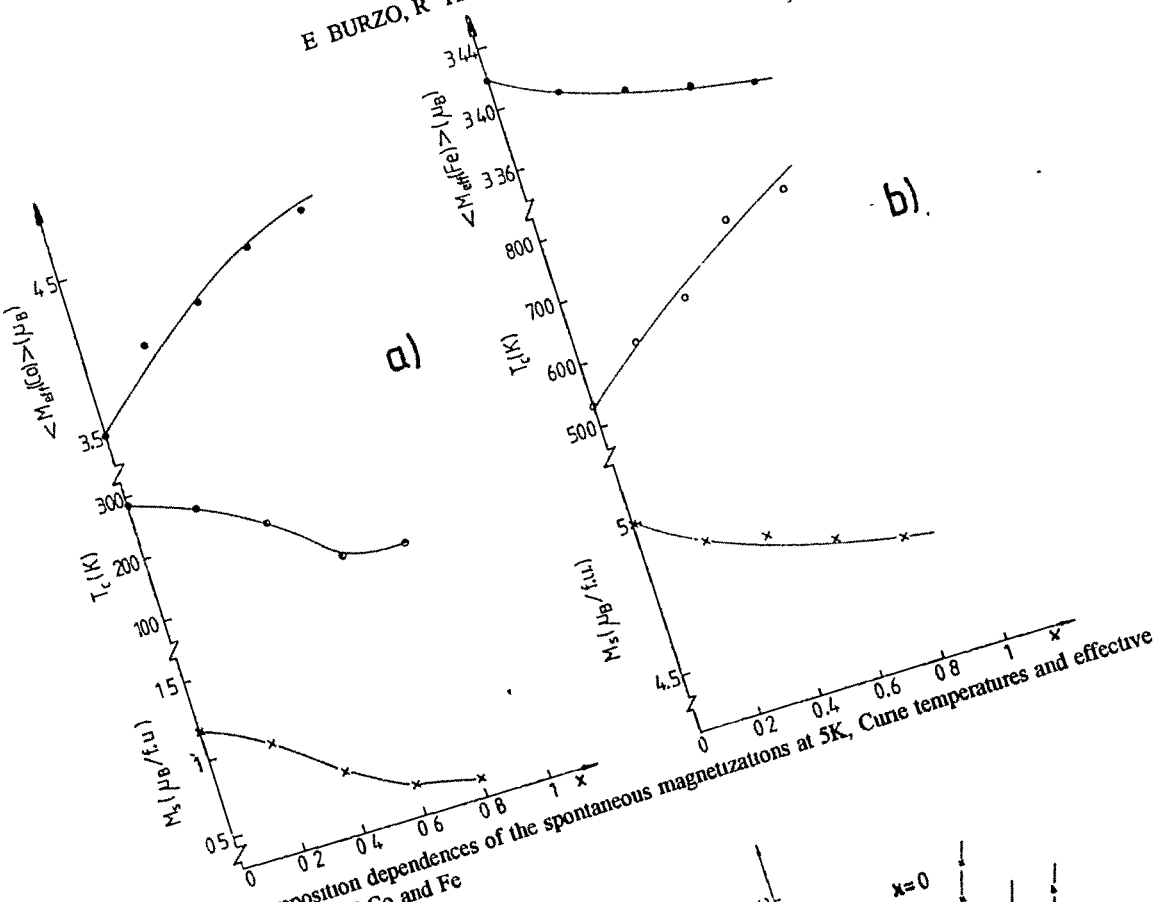

Fig.3. Composition dependences of the spontaneous magnetizations at 5K, Curie temperatures and effective moments of Co and Fe

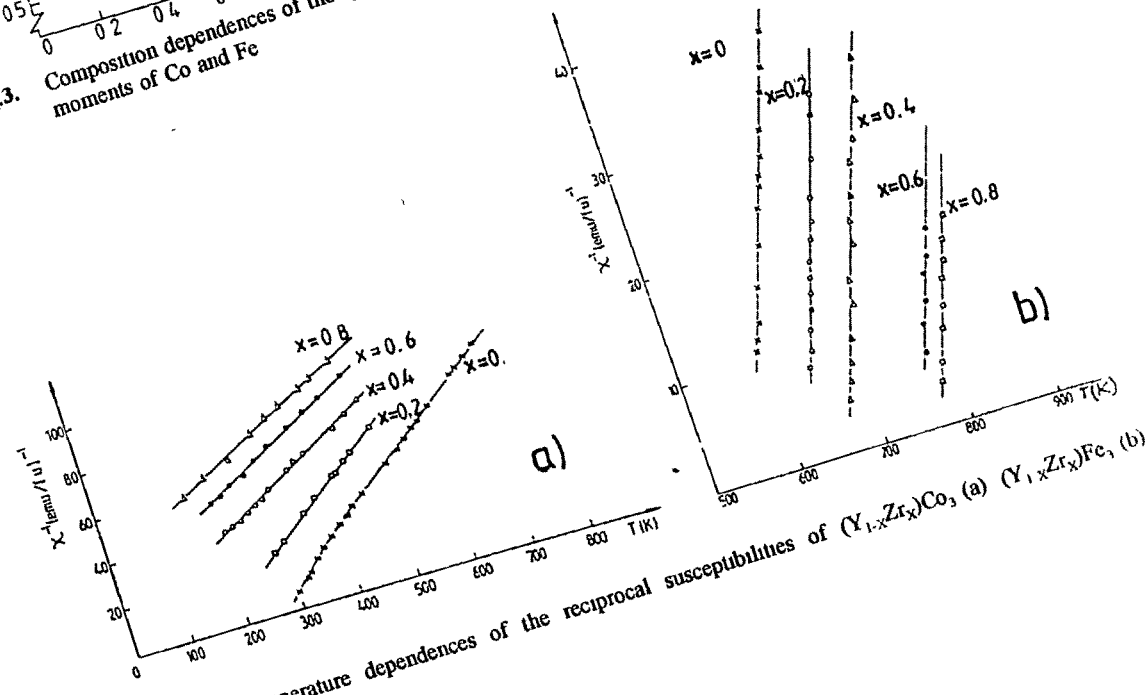

Fig.4. Temperature dependences of the reciprocal susceptibilities of $(Y_{1-x}Zr_x)Co_3$ (a) $(Y_{1-x}Zr_x)Fe_3$ (b) compounds

4. Discussion The mean iron moments, M_{Fe}, in $(Y_{1-X}Zr_X)Fe_3$ system decrease from 1,67 μ_B for x=0 up to 1.56 μ_B (x=0 8) Their variation is around 5% in the studied composition range. The small sensitivity to the composition suggests mainly a localized magnetic behaviour The experimental data may be analyzed in the Stearns model [8] The model supposes that the greatest fraction of iron 3d electrons (95%) are situated in a narow band and can be considered as localized A small fraction of 3d electrons, of the order of 5%, are itinerant contributing to the exchange interaction between localized iron moments

The small decrease of the mean iron moments is accompanied by an increased of the Curie temperature. In order to take into account these data two opposite mechanisms must be considered. The replacement of Y^{3+} by Zr^{4+} increases the electronic concentration of the system. This fact leads to a decrease of the mean iron moments by band filling effects On the other hand, the decrease of lattice constants when increasing zirconium content, determines a diminuation of the distances between iron moments This fact, according to Neel - Slater curve [9] will increase the exchange interaction, Curie temperatures, respectively

Previously [10] we showed that the iron moments in rare-earth compound are little sensitive to the exchange interactions, and only small induced moments appear when increasing exchange interaction, T_c values, respectively Thus , the band filling mechanism predominate, as compared to exchange interactions effects and a small decrease of the iron moment appears, as experimentally observed

A high degree of localization of iron moments is also evidenced by the ratio r= Sp/So between the number of iron spins,Sp, determined from Curie constants and that obtained from saturation moments The r values are of the order of 1 07, close to their limit r = 1, characteristic for a localized moment

As evidenced in Fig 3, cobalt shows a magnetic behaviour, different from that evidenced in case of iron When increasing zirconium content, a high decrease of the mean

cobalt moments and of Curie temperatures is evidenced in $(Y_{1-X}Zr_X)Co_3$ compounds In addition the paramagnetic Curie temperatures change from positive to negative for x=0 37 The ratio r is also strongly dependent on composition, increasing from r=2 for x=0 up to r=9 5 for x=0 8, evidencing a high degree of itinerancy

The magnetic behaviour of cobalt may be analyzed in selfconsistent renormalization theory of spin fluctuations [11] When the amplitude of local spin fluctuations (LFS) is large and fixed, there is a local moment limit, where only the transverse components of LFS are important When the amplitude of LSF is small, there is the weakly ferromagnetic limit where the longitudinal components of LSF play an important role In $(Y_{1-X}Zr_X)Co_3$ system both the transverse and longitudinal components of LSF seem to be present, their relative contribution being dependent on zirconium content

When the local cobalt moment is nil or very weak, as in the above system, the amplitude of LSF can grow rapidly with temperature and are saturated above a certain temperature, higher but close to T_c In $Y_{0\,2}Zr_{0\,8}$ Co_3 the effective cobalt moment is close to those determined for Co^{2+} ions, namely 4 8 μ_B [12] Then the effective moments decrease as the Curie temperatures, exchanges interactions increase This behaviour may be ascribed to a gradual quenching of longitudinal spin fluctuations by the internal field This leads to the diminuation of cobalt effective moments The quenching of spin fluctuations under the action of external field was previously emphasized [13,14] A magnetic field of the order of spin fluctuation temperatures, T_s, ($H_{eff}=k_BT_s/\mu_B\alpha^{1/2}$ where α is the Stoner enhancement factor) is necessary to quench the spin fluctuations enhancement A similar behaviour concerning the quenching of spin fluctuations was previously observed [15,16]

We conclude that $(Y_{1-X}Zr_X)M_3$ compounds with M=Fe or Co, iron shows a localized magnetic behaviour while cobalt is a weak ferromagnet Their magnetic behaviour may be described in different models

REFERENCES

1 Bertaut, E F , Lemaire, R and Schweizer, J ,Bull Soc Tr Mineral Crystallogr **88**, 580, 1965
2 Burzo,E ,Chelkowski,A and Kirchmayr, H.R ,Landolt-Bornstein Handbuch III/19d2, Springer Verlag, 1990
3 Fuji,N ,Pourarian,F and Wallace, W E , J Magn Magn. Mat **24**, 93,1981
4 Kobayachi,K and Kanetmatsu,K ,J Phys Soc. Japan **55**, 4435, 1986
5 Lemaire,R , Cobalt **32**, 132(1966)
6 Givord,D , Givord,F and Lemaire, R ,J Physique **32**, C1-668, 1971
7 Burzo, E and Tetean,R , Solid State Commun **8**, 493, 1993
8 Stearns, M B , Phys Rev **B8**, 4383, 1973
9 Neel,L , Ann Phys **5**, 232, 1936
10 Burzo,E , Solid State Commun **20**, 569, 1975
11 Moriya, T , J Magn Magn Mat **14**, 1, 1979, **100**, 261, 1991
12 Burzo, E , Fizica Fenomenelor Magnetice, vol I Ed Acad , 1979
13 Brunckman, W F and Engelsberg, S , Phys Rev **169**, 417, 1968.
14 Ikeda,K., Gschneidner, K A , Stierman, R, J , Tsang, T W.E and McMasters, O D , Phys Rev **B 29**, 5039, 1984
15 Burzo, E , and Lemaire, R , Solid State Commun. **84**, 1145, 1992
16 Burzo, E , J Magn Magn Mat **140-144**, 2013, 1995

STUDIA UNIV BABEŞ-BOLYAI, PHYSICA, XL, 1, 1995

INFLUENCE OF QUENCHING RATE ON COERCIVE FIELD OF SOFT MAGNETIC POWDERS

I. CHICINAŞ[1], N. JUMATE[1], Gh. MATEI[1]

ABSTRACT. - A correlation of coercive field of soft magnetic powders, obtained by different methods, with grains quenching rate is presented In the quenching rate range 102 - 105 K/s (water pulverization) the coercive field increases by increasing the quenching rate of powders This behaviour is determined by the residual internal stresses When the quenching rate is greater than 106 K/s (rapid quenching onto rotating Cu disk) the coercive field is more reduced as a result of disappearance of crystalline state.

1. INTRODUCTION The coercive field is the most sensitive parameter of the hysterezis loop as a function of the internal structure of the magnetic material, structure which depends on all metallurgical factors which acted on the material during it's elaboration [1] Soft magnetic iron based powders have come back as soft magnetic materials for magnetic cores in electric devices [2,3] In magnetic powders case the coercive field ${}_BH_C$ depends strongly on the residual internal stresses induced during pulverization and on the particle sizes [4-6] For green compacts the coercive field depends on porosity and specific surface of pores [5,7] The heat treatments applied on the powders or on the compacts influence the coercive field also [8].

The quenching conditions strongly influence the crystallization kinetics and consequently the coercive field of magnetic materials [9] Thus, the values of the coercive fields for the amorphous alloys tend to be lower than for related crystalline alloys [10,11]

In this paper earlier results concerning coercive field of soft magnetic powders obtained by different methods [6,12] are correlated by means of powder grains quenching rate

[1] *Technical University, Department of Material Science and Technology, 3400 Cluj-Napoca, Romania*

2. EXPERIMENTAL PROCEDURES Soft magnetic powders from the Fe, Fe-Ni and Fe-Cu-P systems have been produced by three methods water pulverization, gas pulverization, secondary pulverization on the rotating Cu disk These methods ensure a quenching rate of powder grains in the range 10^2-10^7 K/s [13]

The iron powders with 0 04wt% C were elaborated from a 0 37wt% C steel by liquid phase pulverization with water under pressure (80 barr) [4] The Fe-8Ni (wt%) powders were elaborated by water pulverization too The Fe-1.8Cu-0 2P (wt%) powders were elaborated by gas pulverization (Ar at 20-25 barr pressure) and by secondary pulverization on the rotating Cu disk The secondary pulverization on the rotating Cu disk involves re-melting in Ar plasma jet of powders, obtained by Ar pulverization, and projecting of liquid metal droplets on the lateral surface of a rotating Cu disk [12] The rotating Cu disk used for rapid quenching has a 200 mm diameter and a peripheral speed about 31 m/s

The residual internal stresses and the effect of the rapid quenching on grain's size have been evidenced by X-rays diffraction [4,6,12] The coercive fields have been determined from hysteresis loops B-H, which were measured in DC on the green compacts [4]

3. RESULTS AND DISCUSSION It was observed that coercive field ${}_BH_C$ of soft magnetic powders produced by water pulverization (Fe-0 04C and Fe-8Ni, wt%) decrease with increasing powder grain sizes (Fig 1) It was demonstrated [6] that this behaviour of the coercive field ${}_BH_C$ as a function of particle sizes is due to the second order residual internal stresses induced during pulverization

Coercive field of Fe-1 8Cu-0 2P (wt%) powders was reduced from 1400 A/m (powders obtained by Ar pulverization) to 200 A/m by rapid quenching on the rotating Cu disk (fig 2), due to internal structure modification of particles .

Modifications which appear in grains structure by rapid quenching on the rotating Cu disk were examined by X-rays diffraction [12] Total width of diffraction maxima increase

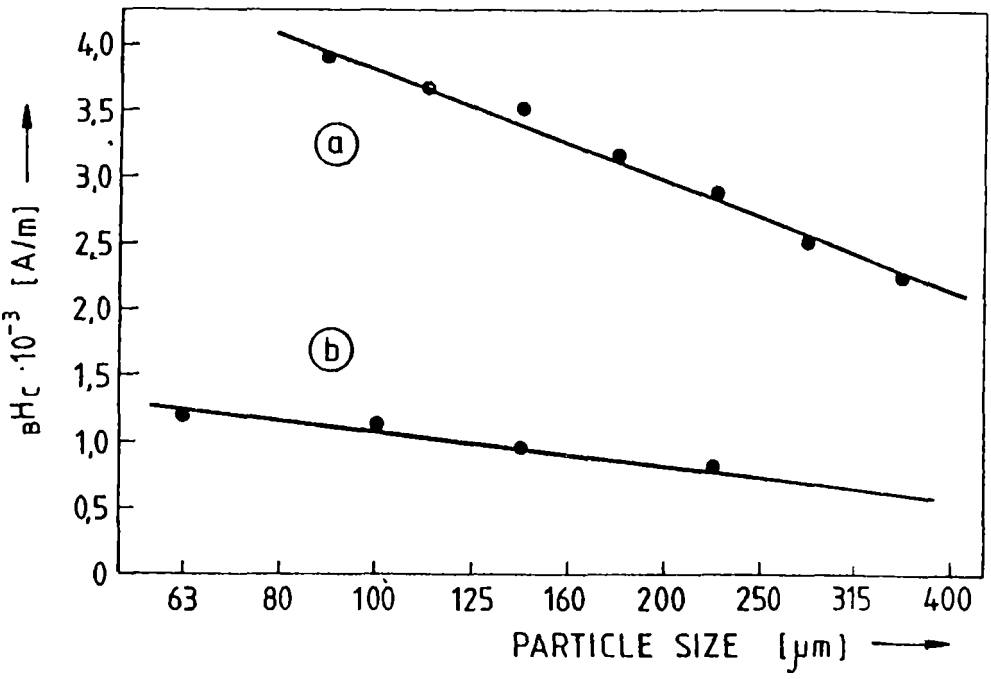

Fig.1. The variation of the coercive field versus particle size (produced by water pulverization) a - Fe-0 04C powders, b - Fe-8Ni powders (wt%)

more for rapidly quenched powders, comparatively with powders obtained by gas pulverization. Thus, in fig 3 is presented the (110) maximum of the solid solution of Cu and P in α-Fe for Fe-Cu-P powders produced by gas pulverization (a) and respectively by secondary pulverization on the rotating Cu disk (b) This suggest a nanocrystalline structure for the powders produced by rapid quenching on the rotating Cu disk, due to the high quenching rate (greater than 106 K/s) It was estimated [12] that the large value of the total width of diffraction maxima for rapidly quenched powders corresponds to a crystalline grains size less than 17 nm Thus, the internal structure of particles explain the behaviour of hysterezis loops showed in Fig 2. The decreasing of the coercive field in the case of nanocrystalline structures may be explained in the random anisotropy model [14-16]

As shown so far, results from fig 1 show the coercive field as a function of quenching rate Assuming that powder grains quenching obtained by water pulverization and by gas

pulverization is made by forced convection (heat transfer by radiation and conduction is neglected) we can write.

$$dQ = kStdt \qquad (1)$$

On the other hand.

$$dQ = mcdt \qquad (2)$$

In these equations dQ is the heat transfer, m - one grain's mass, c - specific heat, dt - temperature variation, k - coefficient of heat transfer by forced convection, S - grain's surface, t - grain's temperature and $d\tau$ - quenching time

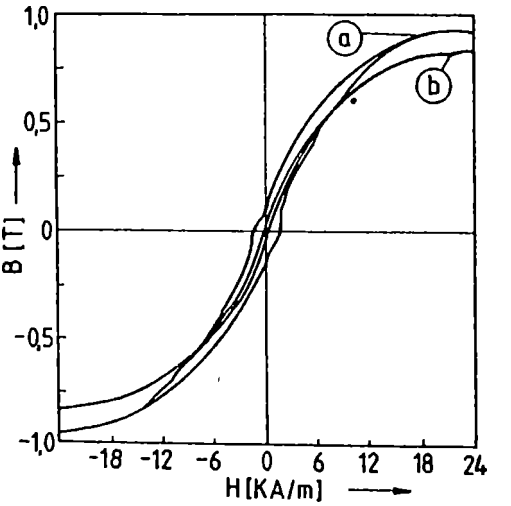

Fig.2. The hyterezis loops of Fe-Cu-P powders produced by. a - gas pulverization, b - rapid quenching

From the equations (1) and (2) results that quenching rate, $dt/d\tau$, is proportional with reciprocal grain's diameter, 1/D

$$\frac{dt}{d\tau} = \frac{6kt}{c\rho}\frac{1}{D} \qquad (3)$$

where ρ is the material density

For water pulverization, grain's quenching rate is in the range 102 - 105 K/s for grains greater than 100 μm [14]

Now, these results (fig 1 and fig 2) will be put together by means of quenching rate (fig 4) Quenching rate range of 105-106 K/s is passing range from residual internal stresses effect to disappearance of crystalline state effect

4. CONCLUSIONS Coercive field of soft magnetic powders as a function of grain sizes and producing method may be analyzed by means of quenching rate In quenching rate

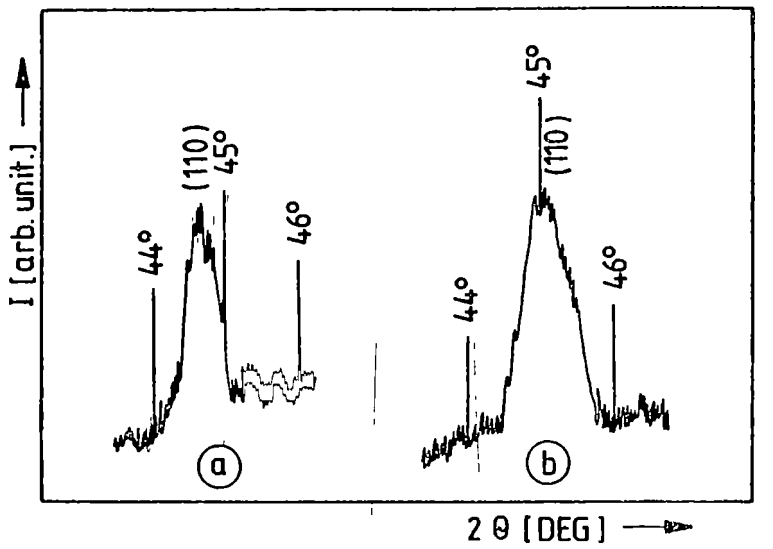

Fig.3. The X-rays diffraction maxima of Fe-Cu-P powders produced by a - gas pulverization, b - rapid quenching

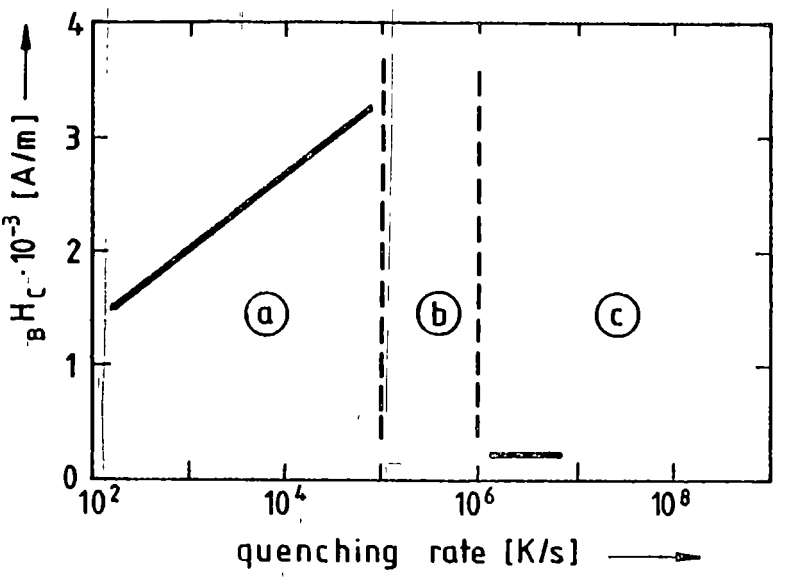

Fig.4. The influence of quenching rate on the coercive field of soft magnetic powders a - internal stresses effect, b - transition range, c - disappearance of the crystalline state effect

range 102-105 K/s (water pulverization and gas pulverization) $_BH_C$ increase by increasing quenching rate of powders This behaviour is determined by second order residual internal stresses When quenching rate is greater than 106 K/s, $_BH_C$ is more reduced as a result of disappearance of crystalline state Further investigations on the 105-106 K/s quenching rate range are necessary

REFERENCES

1. C W Chien, Magnetism and Metallurgy of Soft Magnetic Materials, North-Holand Publishing Company, Amsterdam-New-York-Oxford. 1970
2. B Weglinski, Soft Magnetic PM Materials, in Selected Case Studies in Powder Metallurgy, Ed by I Jenkins and J V Wood, The Institute of Metals, London, 1991, 113-129
3. A Kordecki, B Weglinski, Powder Metall Int **33** (1990), 151
4. Gh Matei, I Chicinaş, N. Jumate, Rom Rep Phys, **46** (1994), 243
5. G. Jangg, M Drozda, G. Eder, H Danninger, Powder Metall Int **16** (1984), 60
6. I Chicinaş, N Jumate, Gh Matei, J Magn Magn Mater, **140-144** (1995), 1875
7. G Jangg, M Drozda, H Danninger, G Eder, Powder Metall. Int. **16** (1984), 264
8. G Jangg, M Drozda, H Danninger, R E Nad, Powder Metall Int, **15** (1983), 173
9. M D. Baró, S Surinach, J A Diego, M T Clavaguera-Mora, N Clavaguera, Mater. Sc & Eng, **A133** (1991), 807
10. F E Luborsky, P.G Frischmann, L A Johnson, J. Magn Magn Mater, **8** (1978), 318
11. F E Luborski, J J Becker, P G Frischmann, L A Johnson, J. Appl Phys, **49** (1978), 1769
12. I Chicinaş, N Jumate, Gh Matei, Rom Rep Phys, (1995), in press
13. N C Grant, Proc. Int Conf Rapid Sol Processing, Reston, Virginia, USA, (1977), 230
14. G Herzer, IEEE Trans Magn **25** (1989), 3327
15. G. Herzer, IEEE trans Magn **26** (1990), 1397
16. G Herzer, Physica Scripta **T49** (1993), 307
17. Randall M German, Powder Metallurgy Science, Copyright 1984, Metal Powder Industries Federation, Princeton New Jersey, p 91

STUDIA UNIV BABEŞ-BOLYAI, PHYSICA, XL, 1, 1995

ESR STUDY OF $xV_2O_5(1-x)[3B_2O_3{\cdot}K_2O]$ GLASSES

D. MANIU[1], I. ARDELEAN[1] and O. COZAR[1]

ABSTRACT. - ESR investigations of $xV_2O_5(1-x)[3B_2O_3{\cdot}K_2O]$ glasses with $0.1 \le x \le 10$ mol% have shown that the V^{4+} ions are present as the isolated species The ESR parameters suggest that the geometry of VO^{2+} complex is distorted from C_{4v} symmetry toward Oh symmetry because of the sixth oxygen atom co-ordinated in the transposition of the vanadyl oxygen The values of MO coefficients indicate an appreciable covalence of the in plane V-O bonds

INTRODUCTION

Vanadyl ion (VO^{2+}) incorporated in glasses as a spectroscopic probe has been measured by several researches [1-12] in order to characterise glass structure The term of "glass structure" involves many particular aspects such as the geometry of structural units of a glass network, the character of chemical bonds in glasses as well as the co-ordination of various transition metallic ions and its change with the composition of glasses

Bogomolova et al [5] and Hosono et al [7] have found two sets of hyperfine structure for vanadyl ions in some phosphate glasses containing Mg, Zn, Be, Cd as modifier cations Also in the case of some sol-gel glasses has been evidenced the presence of three non-equivalent positions (HFS sets) for VO^{2+} ions [12] Toyuki and Akagi [3] pointed out that the ligand field absorption energy $\Delta E = B_{2g} \rightarrow E_{II}^{*}$ of VO^{2+} sensitively reflected the electron-donating ability of ligand oxygen co-ordinating at equatorial position (Oe) of VO^{2+} complex Generally the small variations of the $\tilde{g}$ tensor values ($g_{\parallel}$, $g_{\perp}$) and hyperfine structure constants ($g_{\parallel}$,$g_{\perp}$) with the compositions modification of glasses have been obtained for VO^{2+} ions [11] In the present work, the influence of the V_2O_5 content on the local symmetry and interaction between vanadium ions in potassium-borate glasses has been investigated by ESR measurements

[1] *"Babeş-Bolyai" University, Faculty of Physics, 3400 Cluj-Napoca, Romania*

EXPERIMENTAL

In order to obtain further information on the distributed mode (and magnetic behaviour) of vanadium in oxide glasses, we have investigated the $xV_2O_5(1-x)[3B_2O_3 \cdot K_2O]$ glasses with $0.1 \leq x \leq 10$ mol % maintaining the $3B_2O_3/K_2O$ ratio constant and therefore keeping the matrix structure unmodified

The glasses were obtained by mixing H_3BO_3, K_2CO_3 and V_2O_5 in the desired proportions and then melting this admixture in a sintered corundum crucible at T=1150 °C for 0,5h The molten glasses were poured onto a stainless steel plate The structure of glasses has been studied by X-ray diffraction analysis and did not reveal any crystalline phase

The ESR measurements were performed at 9,4 Ghz (X-band) using a standard JEOL-JES-3B equipment, at the 295K

RESULTS AND DISCUSSION

ESR spectra obtained at room temperature for glasses with small content of V_2O_5 show a well resolved hyperfine structure typical for isolated vanadium ions in a ligand field of C_{4V} symmetry, presented as VO^{2+} species (Fig 1). These are similar to the spectra reported by previous workers [1-14] for vanadium ions in other oxide glasses and may be analysed by using an axial spin Hamiltonian

$$H = \beta_o[g_{II} H_Z S_Z + g_\perp(H_X S_X + H_Y S_Y) + A_{II} S_Z I_Z + A_\perp(S_X I_X + S_Y I_Y)] \qquad (1)$$

Here β_o is the Bohr magneton while g_{II}, $g_\perp$, A_{II}, $A_\perp$ are the components of the $\tilde{g}$ tensor and hyperfine structure tensor, respectively H_X, H_Y, H_Z are the components of the magnetic field , S_X, S_Y, S_Z and I_X, I_Y, I_Z are the components of the spin-operators of the electron and the nucleus, respectively

The magnetic field positions of the parallel and perpendicular hyperfine peaks taking into account the second order perturbation terms, are given by [7,8]

$$H_{\parallel}(m) = H_{\parallel}(0) - mA_{\parallel} - \frac{A_{\perp}^2}{2H_{\parallel}(0)}\left(\frac{63}{4} - m^2\right) \quad (2)$$

$$H_{\perp}(m) = H_{\perp}(0) - mA_{\perp} - \frac{A_{\parallel}^2 + A_{\perp}^2}{4H_{\perp}(0)}\left(\frac{63}{4} - m^2\right) \quad (3)$$

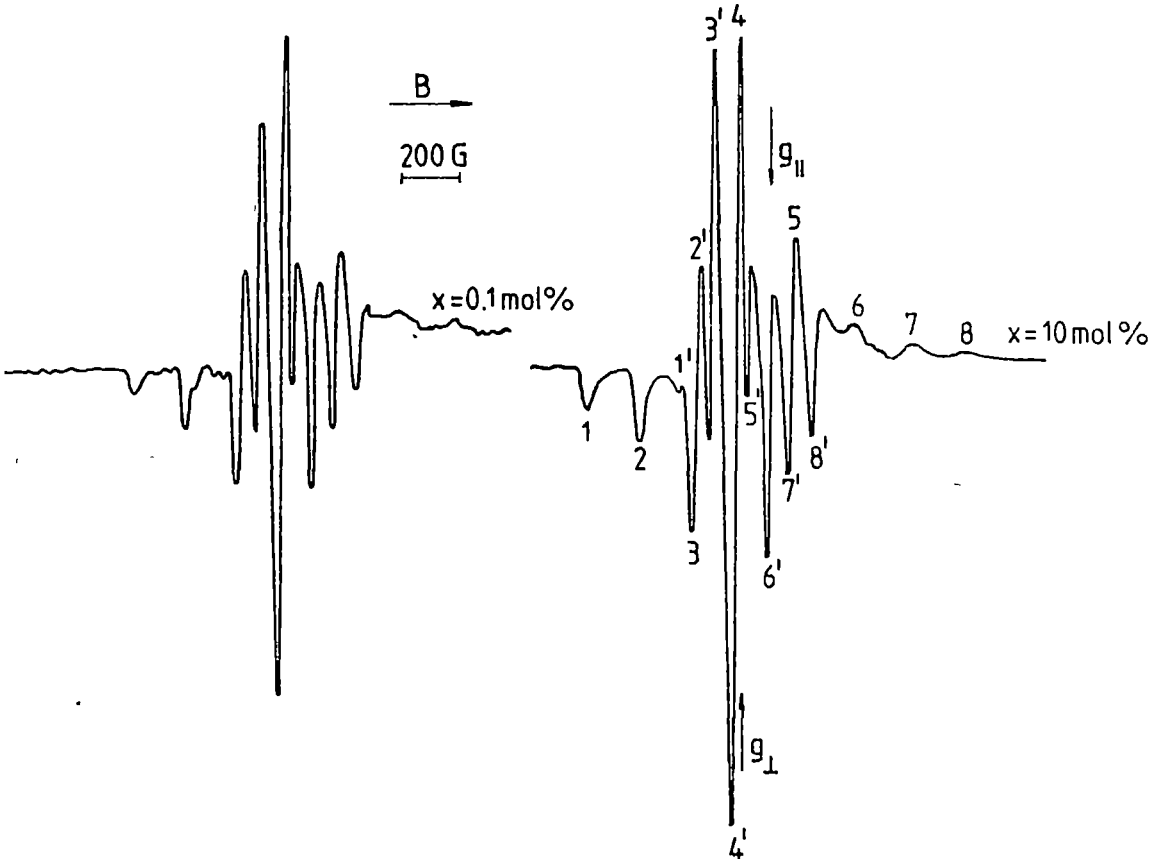

Fig.1. EPR spectra of $xV_2O_5(1-x)[3B_2O_3{\cdot}K_2O]$ glasses at room temperature (1,2,3, and 1',2',3', indicate the parallel and perpendicular HFS peaks respectively)

Here m is the parameters obtained for the studied glasses are given in Table 1 The covalence degrees of the in-plane V-O σ-bonds (β_1^2) and of π-bonding with the vanadyl oxigen ($1-\varepsilon_\pi^2$) were evaluated with the help of LCAO-MO scheme developed by Kivelson and Lee [15] We have taken the spin orbit coupling constant λ=170cm^{-1} [13] and the energy transition

$\Delta_{\parallel}=B_2-B_1^*$ and $\Delta_{\perp}=B_2-E_x^2$ of 16700cm^{-1} and 10500 cm^{-1} respectively [3] The values obtained for (β_1^2), ($1-\varepsilon_x^2$) and Fermi contact (K) parameter are given in Table 1, too

Table 1. ESR Parameters, bonding coefficients and Fermi contact values for studied glasses

x mol %	$g_{\parallel}$	$g_{\perp}$	$A_{\parallel}$ [10^{-4}cm^{-1}]	$A_{\perp}$ [10^{-4}cm^{-1}]	β_1^2	$1-\varepsilon_x^2$	K
0 1	1 944	2 001	171 5	57 6	0 76	0 95	0 72
0 3	1 945	2 002	173 9	57 7	0 75	0 99	0 71
0.5	1 946	2 002	174 1	56 9	0 74	0 99	0 70
1	1 945	2 002	175 3	59 3	0 75	0 99	0 72
3	1 946	2 002	172.9	57.7	0 74	0 99	0 71
5	1.947	2 002	171.5	57 8	0 72	0 99	0 72
10	1 945	2 002	175 9	59 2	0 75	0 99	0 72

The values of the Fermi contact term (K ≈0 72) are smaller than those obtained for other oxide glasses [3,7] This fact shows a great contribution of the 4s orbital of the vanadium atom to the σ bonding orbital (ΨA_1) achieved between vanadium and oxygen ions from the Oz axis [3] On the other hand, the small values of the Fermi contact term (K) suggest [7,15] a decrease of the tetragonality of the $V^{4+}O_5$ complex because of a strongly bonded oxygen atom at V^{4+} ion, in the opposite site of vanadyl oxygen

The values of β_1^2 coefficient show an appreciable covalency degree of the in-plane V-O σ-bonds This fact in the vanadyl group is also consistent with a reduced V-O interaction and an increase of the lenght of this bond, both being related to an increase of the electron donability of the four oxygen atoms coordinated in xOy plane

CONCLUSIONS

The ESR measurements have evidenced the presence of isolated V^{4+} ions in the studied glasses

The small values of the Fermi contact term (K≈0 72) suggest a hexacoordinated

geometry of the oxovanadium complex near octahedral (Oh) symmetry because of the reduction of the V-O interaction in the vanadyl group caused by a strong axial perturbation arising from the sixth oxygen atom coordinated in the transposition to the vanadyl oxygen

The values of MO coefficients indicate an appreciable covalency of the in plane V-O σ-bonds in agreement with the proposed local symetry at V^{4+} ion site

REFERENCES

1 G Hochstrasser, Phys Chem Glasses, 7, **178**(1966)
2 H G Hecht, T S Johnston, J Chem. Phys 46, **23**(1967)
3 H Toyuki, S Akagi, Phys Chem Glasses, 13, **15**(1972)
4 A Paul, F Assabghy, J Mater Sci 10, **613**(1975).
5 L D Bogomolova, V.N Jackin, V N Lazukin, T K Pavlushkina, V.A.Shmuckler, J Non-Cryst Solids 28, **375**(1978)
6 H Hosono, H Kawazoe, T Kanazawa, J.Non-Cryst Solids 33, **125**(1979)
7 H Hosono, H Kawazoe, T Kanazawa, J Non-Cryst Solids 37, **427**(1980)
8 J M Dance, J P Darmaudery, H Bandry, M.Monnereraye, Solid State Commun, 39, **199**(1981)
9 O Cozar, I Ardelean, Gh.Ilonca, Mater Chemistry, 7, **155**(1982)
10 O Cozar, I Ardelean, I Bratu, Gh Ilonca, S Simon, Studia Babeş-Bolyai 2, **94**(1989)
11 V P Seth, S Gupta, A Jindal, S K Gupta, J Non-Cryst Solids, 162, **263**(1993)
12 A Shamers, O Lev, B Iosefzon-Kuyavskaya, J Non-Cryst Solids, 163, **105**(1993)
13 I Ardelean, O Cozar, Gh Ilonca, J Non-Cryst Solids, 68, **33**(1984)
14 O Cozar, I.Ardelean, Gh.Ilonca, Gh.Cristea, Rev Roum Phys 33, **1125**(1988)
15 D Kivelson, S K Lee, J Chem Phys 41, **1896**(1964)
16 D Manu, I Ardelean, T Iliescu, Mat Lett 25, **147**(1995)

STUDIA UNIV BABEŞ-BOLYAI, PHYSICA, XL, 1, 1995

RESEARCH ON ILMENITE POWDER PROCESSING IN PLASMA JET

I. BICA[1] and T. CHEVEREŞAN[2]

ABSTRACT. - The paper presents the main mechanism and processes which take place at ilmenite powder dissociation in plasma, equipment designed for plasma metallurgy of metalliferous powder plasma respectively experimental results

Introduction. Using thermic plasma enables production of new materials as multicomponent particles [1], fine and ultrafine particles [2,3,4], refractors & composite material [5], obtaining surfaces see [7] respectively superconducting materials [8,9]

On the other hand, plasma is useful as we shall shows as follows, for extracting of materials from metalliferous powders

That occurs by thermic dissociation of compounds of that particular metal, obtaining, by fast cooling easy processing metal or compounds

Thermic dissociation of ilmenite. Ilmenite powder ($FeTiO_3$) dissociates at a temperature T,pursuant to relation (1)

$$FeTiO_3 \rightleftharpoons Fe_{(l)} + Ti_{(s)} + \frac{3}{2}O_2 \qquad (1)$$

Variation of free enthalpy ΔG, for the reaction (1) has the value [10] (eq 2)

$$\Delta G = 1376800 + 170\,5 \cdot T \cdot lg(T) - 0\,8 \cdot 10^{-3} \cdot T^2 + \frac{5\,8 \cdot 10^5}{T} - 633\,18 \cdot T \qquad (2)$$

For temperatures $T \geq 3300$ k [10], the reaction (1) strongly displaced toward right Principal sketch of the plasma generator designed for thermic dissociation of ilmenite is shown in fig 1

---

[1] *University of Timişoara, Department of Physics, 1900 Timişoara, Romania*

[2] *TES SA Plasma Department, 1900 Timişoara, Romania*

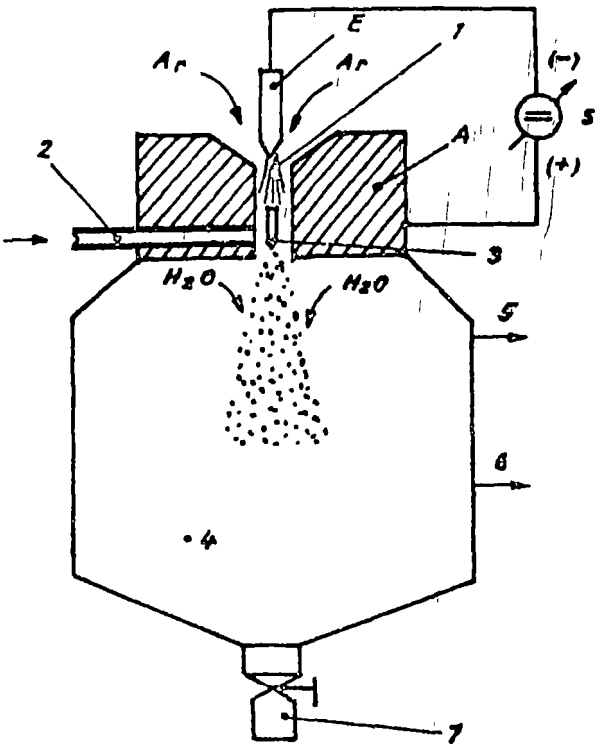

Fig.1 Plasma generator designed for metalliferous powder metallurgy (Principal sketch)

The current source S feeds the electric arc 1, in start argon medium between the electrode E and nozzle A of the plasma generator Under argon pressure, the plasma of the electric arc is dawn toward the exterior of the nozzle

The ilmenite powder, at constant flow rate and well chosen granulation, under plasmagenous gas (argon, air, etc) pressure is dawn through tube 2 into the plasma jet 3

At plasma jet temperatures in the range of 5000 K 20000 K there takes place the ilmenite thermic dissociation reaction The obtained product is cooled up by a water jet and collected in chamber 4

Residual gases are eliminated through pipe 5, water surplus through pipe 6 The powder in chamber 4 is collected by valve tube 7 The speed v_j of argon plasma jet is adjustable by discharge current intensity I [11]

$$V = \frac{3 \cdot \mu_o \cdot I^2}{64 \cdot \pi^2 \cdot \eta \cdot r_o} \tag{3}$$

where - η dynamic viscosity of plasma Kg/ms

- r_o effective radius of plasma cylinder, m

- m_o magnetic permeability of vacuum

For argon at 10^4 K,η = 1 84 10^{-4} Kg/ms and respectively for r_o = 3 10^{-3} m, we obtain by expression (3) the plasma jet speed of up to 3800 m/s (fig 2)

The Reynolds criterium for the jet diameter d = 8 10^{-3} m and kinematic viscosity coefficient of argon plasma ν = 0 92·10^{-2}m/s takes values in the range Re = 700-3200 (fig 2)

The plasma jet flow being laminary (Re < 10^4) it yields that plasma temperature distribution [11] is described by the function

$$T = \frac{(2 \cdot P_r + 1) \cdot Q}{8 \cdot \pi \cdot \eta \cdot C_p \cdot L} + \left(\frac{c}{1 + c - \lambda}\right)^{2P_r} \tag{4}$$

where - $P_r = P_r = \frac{\eta \cdot C_p}{k}$ - Prandtl criterium

- C_p specific heat of plasma J/KgK

- k conductibility of plasma J/(ms·K)

- Q plasma jet power, W

- L plasma jet length, m

- c, λ constants

For argon plasma jet at 10^4 K [11] C_p = 10^3 J/kgK}, k = 0 68 J/msK and ρ = 2·10^{-2} kg/m^3 At powers P = 6 10^4 W in the electric arc the conversion efficiency factor experimentally determined, as about 0 2 As a consequence the plasma jet power is Q = 12000 W Temperature distribution in the plasma jet is shown in (fig 3) It could be observed that temperatures in plasma jet rank between 1264K-37320 K

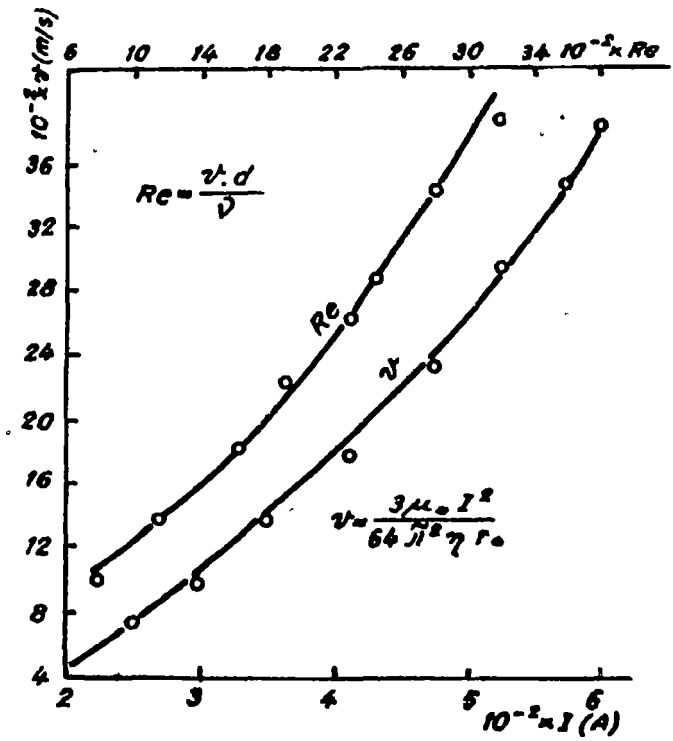

Fig.2 . Speed v_j of the plasma jet and, respectively, of the Reynolds criterium as a function of the intensity of the discharge current in argon medium

The metalliferous powder particle goes in the plasma a distance of length l, which has the value, in case $R_e > 2$ [6,5] given by eq (5).

$$l = v \cdot [t - t' \cdot \ln(1 + \frac{t}{t'})] \tag{5}$$

The space l is passed by the particle with the speed given by eq (6),where t is the time in s

$$V_p = \frac{v \cdot t}{t' + t} \tag{6}$$

The time t' is determined from the expression [5,6].

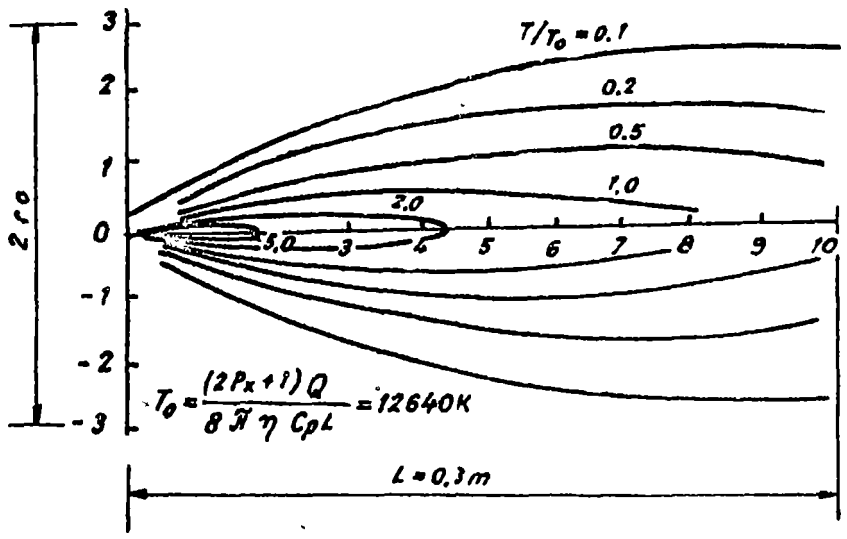

Fig.3 Temperature T distribution along the plasma jet

$$t' = \frac{4 \cdot d_p \cdot \nu}{3 \cdot \psi \cdot v \cdot \rho} \tag{7}$$

where - d_p particle diameter in m

- ψ drag coefficient for particle movement in plasma

For values I > 200 A, the coefficient is determined from expression [11]

$$\psi = \frac{6\pi}{R_e}\left(1 + \frac{3}{8}R_e\right) \tag{8}$$

For $d_p = 1 \cdot 10^{-3}$ m, v = 2600 m/s, ψ = 7 07, $\nu = 0\ 92 \cdot 10^{-2}$ m^2/s and $\rho = 2 \cdot 10^{-2}$ $kg \cdot m^{-3}$ we obtain from (7) that t' = 0 83 ns

Time variation of l and v_p, determined with (5) respectively with (6) are shown in (fig 3) There could be observed from (fig 3) that in the time intervalof 10 ns, the speed of the particle becomes equally to that of the plasma, the length way gone passed by the particle is $l = 3\ 5 \cdot 10^{-3}$m Because of ilmenite powder only the iron component is important, we shall present further only this component

At iron particle heating in argon plasma, the BIOT criterium is smaller than the unit [5] (Bi = 0 01)

Because of that reason the particle temperature T_p in argon plasma jet is evaluated by the relation [5]

$$T_p = T - (T - T_{po}) \cdot \exp(-\frac{t}{t''}) \tag{9}$$

where - T_{po} initial particle temperature, K

The time t" is evaluated from relation (10) [5]

$$t'' = \frac{c' \cdot \rho_p \cdot d_p}{6 \cdot \alpha} \tag{10}$$

where - c' specific heat of particle, J/ Kg K

- ρ_p particle density Kg /m^3

- α convection coefficient J / m^3sK

For iron particles in melted state [11] c'= $89 \cdot 10^{-4}$, ρ_p= $6\,5 \cdot 10^3$ kg/m^3 and respectively for the average convection coefficient $\alpha = 16\,72 \cdot 10^4$ J/m^2sK results of (10) and t''= 23 1 ns

Time variation of temperature T_p evaluated from (9) is shown in (fig 4) There is observed of (fig 4) that for plasma jet speed v = 2600 m/s, ilmenite particles reach in 10 ns time intervals the temperatures of 3800 K (curve 1) respectively temperatures of 10000 K (curve 2) T_p temperature values is determined by the area of plasma jet (fig 3) in which ilmenite powder arises

Experimentally, obtaining of ilmenite power dissociation conditions has been performed using the plasma generator shown in (fig 1) completed with the additional nozzle A_1 and cylinder anode A_2 (fig 5)

The source S_1 feeds the electric discharge between thr electiode E and the nozzle A

The source S_2 maintains the electric discharge between the electrode E and the anode A2

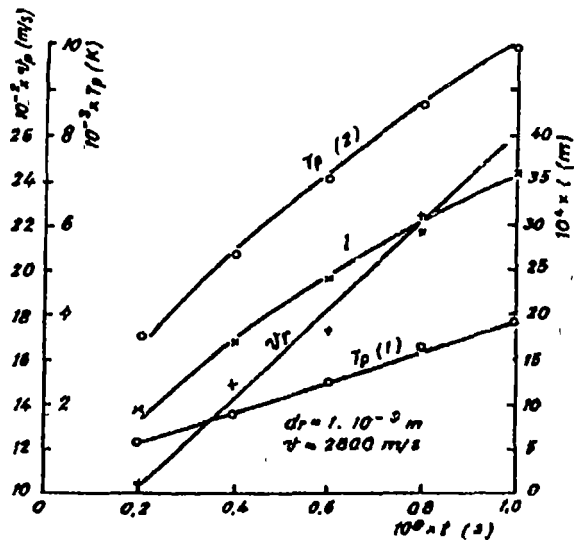

Fig.4 · Speed v_p , temperature T_p and length l gone by the particle in the plasma jet as a function of time t. (1) T= 10000K, (2) T=25000 K,

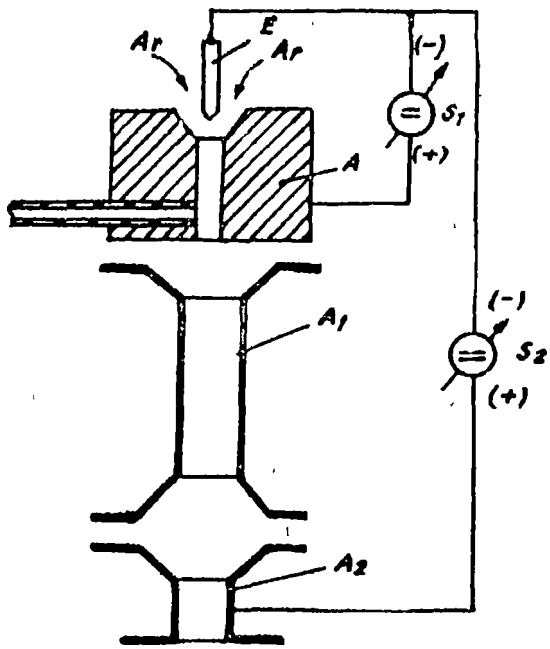

Fig.5 Plasma generator design for thermic dissociation of ilemnite powder

Experimental results. Physical building of plasma generator of (fig 5) in shown in (fig 6) It allows obtaining a plasma jet with a length of up to L = 0 25 0 3 m in argon or argon mixed with nitrogen

In continuous duty the power of the electric arc is up to 60000 W Raw material on which plasma jet evaluating experiments have been performed originates from titaniferous alluvions of subcarpatian zones of the Arges district (Merisem, Borlesti) Mineralogical composition of ilmenite concentrate is as follows

Ilmenite ($FeTiO_3$)	80 0%
Titanomagnetice ($FeTiO_3$ Fe_3O_4)	5 0%
Rutil (TiO_2	1 0%
Oligist	0 5%
Quartz, Silicates	13 0%

Table 1:

Mineralogical Composition(%)	Arc Power($10^{-3} \times P(W)$)								Remarks
	20	30	35*	40*	45*	50*	55*	60*	
Ilmenite powder	-	10	-	15	20	-	-	-	*Plasmagenous gas Ar+20%N_2
Ilmenite globular	60	80	55	-	-	50	20	-	
Ilmenite μ-globular	-	-	-	55	50	-	-	-	
Ilmenite powder pressed	-	-	-	-	-	-	-	17	
Ilmenite sinter	40	-	25	-	-	20	-	-	
Hematite	-	-	5	-	-	5	5	3	
Limonite	-	10	10	-	25	-	15	10	
Ferrite	-	-	5	-	5	-	-	-	
Dendrite Ferrite	-	-	-	-	-	-	50	70	
Globular Ferrite	-	-	-	5	-	-	-	-	
Limonite	-	-	-	-	-	15	-	-	
Coloidal Limonite	-	-	-	25	-	-	-	-	
Drop& Dendrite Ferrite	-	-	-	-	-	10	-	-	
Copper-coming from plasma generator nozzle(incidental)	-	-	-	-	-	-	10	-	

Fig.6 · Plasma generator build for plasma jet dissociation of metallipherous powder

Table 2.

	Arc Power($10^{-3} \times P(W)$)								Remarks
	20	30	35	40	45	50	55	60	
α (%)	0	10	45	50	50	60	90	95	
Fe (%)	0	6	13	14	15	20	60	75	

Powdered raw material has granulation between 0 1·10^{-3}m and 1 5·10^{-3} m Carrier gas used is argon (0,17·10^{-3} m^3/s) Ilmenite powder flow rate has been kept constant (28·10^{-2} kg/s) Plasmagenous gas flow rate is 0 50·10^{-3} m^3/s

Experimental research had as tasks

· Determination of power (P) in the electric arc due to which the thermic dissociation ofilmenite power occurs

· Determination of mineralogical composition of the powder passed through plasma jet

· Determination of the dissociation degree of $FeTiO_3$ in plasma jet, respectively

· Estimation of iron concentration in ilmenite lattice [Fe%]

The obtained experimental results are shown in table 1, respectively in table 2

Referring to tables 1 and 2 we could mention as follows thermic dissociation of ilmenite begins from powers in the electric arc of 30000 W At powers of 60000 W, $FeTiO_3$ has been dissociated at a level od 95%, 75% of the iron having been extracted from ilmenite lattice

The remained titaniferous mass is titanium strongly enriched, therefore it could be proceeded to direct titanium tetrachloride production

Conclusions. Plasma jet is the placement of high temperatures 10^4 3·10^4 K and a distribution as shown in (fig 3)

Plasma jet speed determined by discharge current intensity is shown in (fig 4) In 10 ns time intervals $FeTiO_3$ particles reach thermic dissociation temperatures (fig 4)

Thermic dissociation of ilmenite powder used begins from powers in the electric arc of 30000W At powers of 60000 W, in argon and 20\% nitrogen medium, the thermic dissociation degree of $FeTiO_3$ has level of 95\%.

We consider that at discharge current intensities $I \geq 600$ A and in $Ar+H_2$ (or $Ar+CH_4$) medium the iron concentration dislocated from ilmenite lattice may exceed 75% (as it is at present)

The secondary product (60% -80% TiO_2) may serve for direct titanium tetrachloride production

REFERENCES

1 Li Z - PhD Thesis, Technical University in Aachen (1990)
2 Bica I - Doctoral Thesis, University in Timisoara (1991)
3 Bica I - Sixth International Conference On Magnetic Fluids, Paris 1992, Proceedings, page 230-231
4 Bica I - Magnetohydrodynamics (Riga) 1 (1994) 121 - 122
5 Uda M - Nanostructured Materials 1 101 - 106 (1992)
6 Rykalin N N - Pure and Appl Chem 48, 179-194 (1976)
7 Rykalin N N Kudinov V.Y - Pure and Appl Chem 48, 229-239 (1976)
8 Suhr H - Pure and Appl Chem 39, 335-415 (1974)
9 Ohmori A Sand S Arata Y - Transactions of JWRI 20, 1, 53-61 (1991)
10 Ohmori A Zhou Z , Suzumura A Arata Y - Transaction of KWRI, 1, 107-113 (1990)
11 Oprea Fl - Teoria Proceselor Metalurgice, Ed Didactică şi Pedagogică, Bucureşti
12 Lancaster J F - The Physics of Welding, Pergamon Press Oxford (1984)

STUDIA UNIV BABEŞ-BOLYAI, PHYSICA, XL, 1, 1995

ON THE FORMATION OF GRAPHITE NANOPARTICLES IN ARGON PLASMA

I. BICA[1]

ABSTRACT. - The paper presents the main mechanisms for obtaining graphite nanoparticles of 2-ethyl-hexyl-iron maleat by plasma jet dissociation

Results. The Argon plasma jet obtained in specialized plasma generators [1,2,3,4] is the origin of high value action energies Temperatures obtained in argon plasma jets [1] initiate the thermic dissociation of 2-ethyl-hexyl-iron maleat jet sprayed in argon[1]

$$Fe[OOC-CH=CH-COO-(CH_2)_4-\underset{\displaystyle C_2H_5}{\underset{|}{CH}}-CH_3]\rightarrow Fe=C+H_2O\begin{matrix}O_2\\ /\\ \\ \backslash\\ H_2\end{matrix} \qquad (1)$$

In the interface of 2-ethyl-hexyl-iron maleat jet-plasma there is formed a heterophase system

The appearance probability of the heterophase system is

$$P = A\cdot\exp\left(-\frac{\Delta G}{kT}\right) \qquad (2)$$

where

A-proportionality coefficient,

ΔG- free system enthalpy variation,

k-Boltzmann's constant,

T-temperature of the system,

[1] *University of Timişoara, Department of Physics, 1900 Timişoara, Romania*

The variation of the free enthalpy of the system is [6]

$$\Delta G = (\mu_2 - \mu_1)n + \gamma\alpha n^{\frac{2}{3}} \tag{3}$$

where

n-number of atoms in the surface layer,

γ-surface tension,

μ_2- chemical potential of pure state substance,

μ_1- chemical potential of carbon in 2-ethyl-hexyl-iron maleat solution,

The magnitude α is a geometrical shape factor intervening in the expression of the nucleus surface S

$$S = \alpha n^{\frac{2}{3}} \tag{4}$$

At an energy equal to the minimal free enthalpy, the nucleus formation process activates In this case the critical number of atoms for which the nucleus becomes stable is

$$n_{cr} = \frac{8}{27}\frac{d^3\gamma^3}{(\mu_1-\mu_2)^3} \tag{5}$$

which is corresponding to

$$\Delta G_{max} = \frac{4}{27}\frac{d^3\gamma^3}{(\mu_1-\mu_2)^2} \tag{6}$$

The constant of the nucleus increasing speed is minimal and has the value

$$K_{max} = c\cdot\exp\left[-\frac{2\beta T_0^2}{k(T_0-T_1)^3}\right] \tag{7}$$

where c is a constant when the optimal temperature T_1 can not be less than $1/3\cdot T_0$

In that case the activation energy is

$$\frac{E}{\beta} = \frac{T_0^2}{(T_0 - T_1)^3}(3T_1 - T_0) \tag{8}$$

where T_1, T_0 are the optimal and respectively initial system temperatures

The magnitude β is a notation

$$\beta = \frac{4}{27}\frac{d^3\gamma^3}{(\Delta H)^3}$$

where ΔH is th molar enthalpy developed during phase transformations

We assume further that the crystal nucleus is of cubic shape Its growing is due to the deposit of n atoms on each surface of the cube In this case the appearing of system bidimensional fluctuations is accompanied by free enthalpy variation

$$\Delta G' = (\mu_2 - \mu_1)n + \alpha_l \gamma' n^{\frac{1}{2}} \tag{9}$$

where

μ_1, μ_2 -chemical potentials of old respectively new phase,

α_l- a numeric coefficient,

γ'-linear tension,

l-perimeter of a surface of a cube shaped nucleus,

The growing of the bidimensional nucleus occurs with a high speed until the maximal value of free energy

$$\Delta G''_{max} = \frac{3}{4}\frac{d_l^2 \gamma'^2}{\mu_1 - \mu_2} \tag{10}$$

The value for the expression (10) corresponds to a critical number of atoms of the bidimensional nucleus, that is

The growing speed constant for the bidimensional nucleus is maximal and has the

$$n'_{cr} = \frac{\alpha_l \gamma'^2}{4(\mu_1 - \mu_2)^2} \tag{11}$$

value

$$K'_{max} = c' \exp\left(-\frac{\beta' T'_0 T_2}{kT_2(T_2 - T'_0)^2}\right) \tag{12}$$

when the following condition is met

$$\frac{2T_2 - T'_0}{(T_2 - T'_0)^2} = -\frac{E'}{\beta' T'_0} \tag{13}$$

The value β from (12) and (13) is a notation

$$\beta' = \frac{3\alpha_l^2 \gamma'^2}{4\Delta H'}$$

where ΔH' is a molar enthalpy developed during phase transformations specific for bidimensional nucleus growing

From (13) it could be observed that the temperature T_2 can not be less that $T'_0/2$ Meeting the condition (6) of crystal nuclei activation and respectively of equation (13) are integrally fulfilled in plasma jet

So, at a flow rate of 2 ml/min of 2-ethyl-hexyl-iron maleat at plasma jet parameters corresponding to data shown in Fig 1, there have been obtained nanoparticles (Fig 2)

The granulation of obtained particles is between 30 Å and 100 Å, with an average of 63 Å

Dimensional control of nanoparticles has been performed of the 2-ethyl-hexyl-iron maleat quantity introduced in argon plasma So, at a 2-ethyl-hexyl-iron maleat flow rate of 6ml/min, particle granulation increased with about 80%, comparing to that presented in fig 3

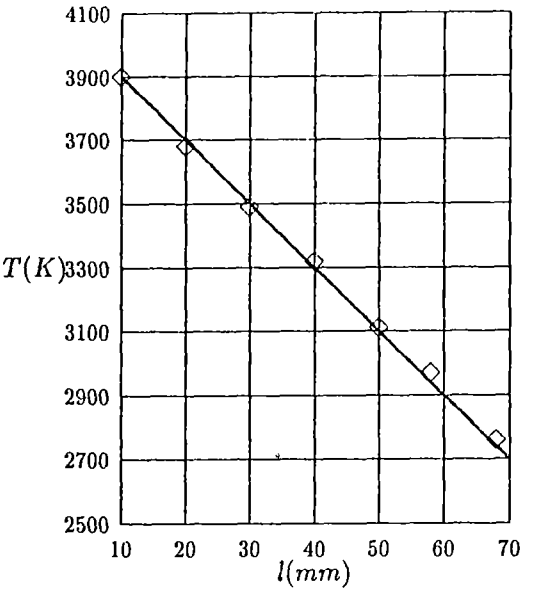

Fig.1. Temperature distribution of the plasma jet along the length l of the plasma jet (gas argon 10 l/min, carrier gas argon 15 l/min, arc U=100V_{ac}, I=80A_{ac}, nozzle diameter d=8mm

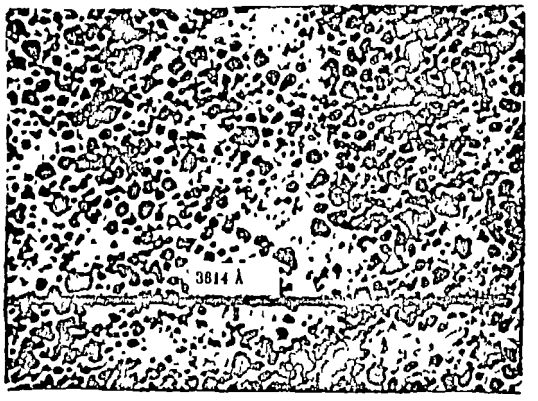

Fig.2. Graphite monoparticles (×207500)

The obtained powder is collected in 2-ethyl-hexyl-sodium-sulphosuccinate The temperature of the collecting liquid is maintained at the level 353 K ± 20%

The iron in 2-ethyl-hexyl-iron maleat ia a mass ratio of 1/5 is transformed into ultrafine particles

At pressures of $6 \cdot 10^5$, a part of the iron ultrafine particles are deposited on the walls

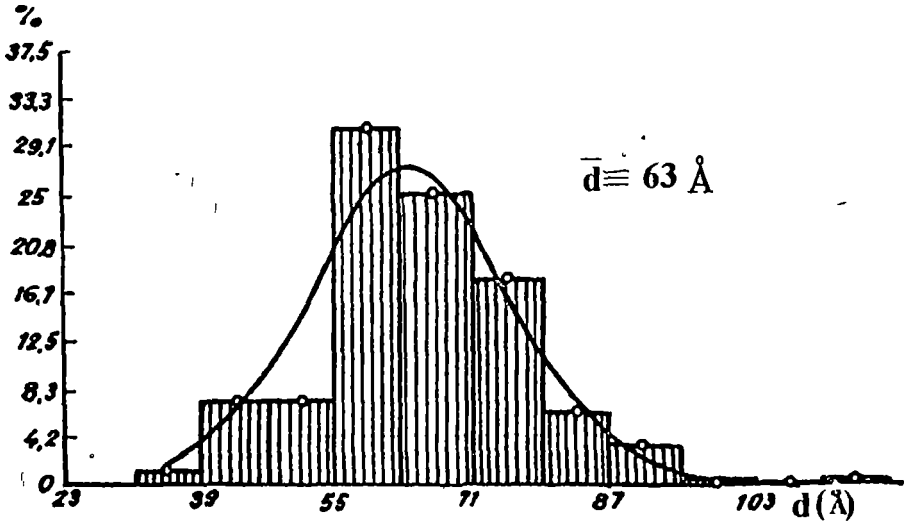

Fig.3. Histogram of the graphite particles

of the power collecting chamber while another part is drawn by residual passes toward the

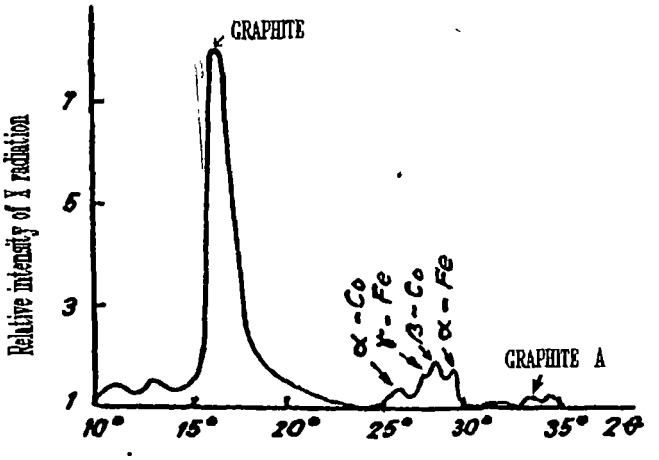

Fig.4. Roentgenogram of graphite particles

The cooling speed of 160000 K/s obtained in the plasma jet makes it possible, to obtain, besides crystal graphite (G C) also amorphous graphite (G A) (fig 4)

Conclusions. Plasma jet thermally dissociates 2-ethyl-hexyl-iron maleat Temperature distribution of the argon plasma jet, as well as its energy, lead to fulfill the condition (8) of nuclei activation respectively to satisfying of condition (13) on graphite particles growing

Under identical energetic conditions of plasma jet, dimensional control of particles is performed from material flow rate introduced to plasma

Material cooling speed of 160000K/s leads to obtaining, besides crystal graphite also amorphous graphite

Acknowledgements. The paper has been prepared with financial aid of the Research Institute for Condensed Matter, Str. Tîrnava 1, Timişoara

REFERENCES

[1] Bica, I - Doctoral Thesis, University of Timisoara, 1991
[2] Bica, I - VI-th Int Conf On Magn Fluids, Paris 1992, Proceedings, p.230-231
[3] Bica, I ,Bica, D -Magnetohydrodynamics ,1, Riga 1994
[4] Bica, I - Research on Nanoparticles Obtaining (to be published)
[5] Bica, I - Obtaining of Nanoparticles in Argon Plasma (to be published)
[6] Oprea, Fl ,Theory of Metallurgial Process, Didactical and Pedagogical Pub House, Bucharest, 1984

STUDIA UNIV BABEŞ-BOLYAI PHYSICA XL, 1, 1995

ENHANCEMENT OF THE DIFFUSION PROCESSES IN AGAR GEL FOLLOWING THE ULTRASONIC PRETREATMENT OF CERTAIN CHLORIDE SALTS

Eva VERESS[1], K. PETHŐ[1] and C. TARBA[1]

ABSTRACT. - Ultrasonic irradiation (1W/cm^2, 1MHz) of 0 1N $SrCl_2$ or $BaCl_2$ solution for variable periods (5, 10, and 15 min) resulted in a saturating dose and time dependent acceleration of the diffusion processes in the agar gel These characteristics and the fact that the values observed are higher for Ba^{2+} than for Sr^{2+} suggest as a likely explanation of the ultrasound action the depleting effect on the hydration shells of the two ions, the hydrated radius of Ba^{2+} being smaller than that of Sr^{2+}

Introduction The object of the present paper is the study of ion transport in agar gel following the ultrasonic treatment of rather dilute (0 1N) solutions of $SrCl_2$ and $BaCl_2$ The agar gel may be considered as a model system for the cytoplasm, having a characteristic phylamentous structure which is able to retain an appreciable amount of salt solutions The migration of the chloride salts in the gel is revealed by the precipitation with $AgNO_3$

Acceleration of the transport phenomena through different biological materials, especially membranes, with the aid of the ultrasounds has been a major subject of study lately [1,2] However, such studies were always performed by exposing the entire system (membrane and solution), or just the membrane to ultrasonic irradiation By our knowledge, the present study is the first in which only the salt solution is treated with ultrasounds and which demonstrates that such a treatment results in the enhancement of the diffusion of certain chloride salts in agar gel An additional original fact is a technical improvement of the method that will be described below

[1] *"Babeş-Bolyai" University, Faculty of Biologie, 3400 Cluj-Napoca, Romania*

Experimental method

Preparation of the agar gel

A quantity of 1 8 g agar is dissolved in 100 ml distilled water by warming the mixture on a water bath After the filtration through a filter paper, 10 ml of a 0 1N $AgNO_3$ are added to the mixture

Volumes of 1 3 ml of the preparation thus obtained are distributed in mm-graduated Westergreen pipettes, held in a stative, kept in dark to avoid the photochemical reactions, and used after 24 hours

Ultrasonic treatment of the solutions

The freshly prepared solutions of $SrCl_2$ and $BaCl_2$ (0 1N) were submitted to 1 MHz ultrasounds obtained from a TESLA piezoelectric generator, at an intensity of 1 W/cm^2 The waves were directed vertically, against the gravitational force and generated continuously for variable treatment durations 5, 10 and 15 min During treatment the solution samples were thermostated at 16^0 C

Measurement of the diffusion velocity and conductance

An equal quantity (1 ml) of either treated or untreated (control) solutions were introduced on the top of the agar gels found in the Westergreen pipettes and the diffusion process was followed for 3 hrs, with readings at every 20 min

The total mass of ions diffused at different time intervals was calculated from the dimensions of the gel column penertated by the solution (as visualised by the silver precipitate)

The conductance of the solutions was measured with a Radelkis OK 10211

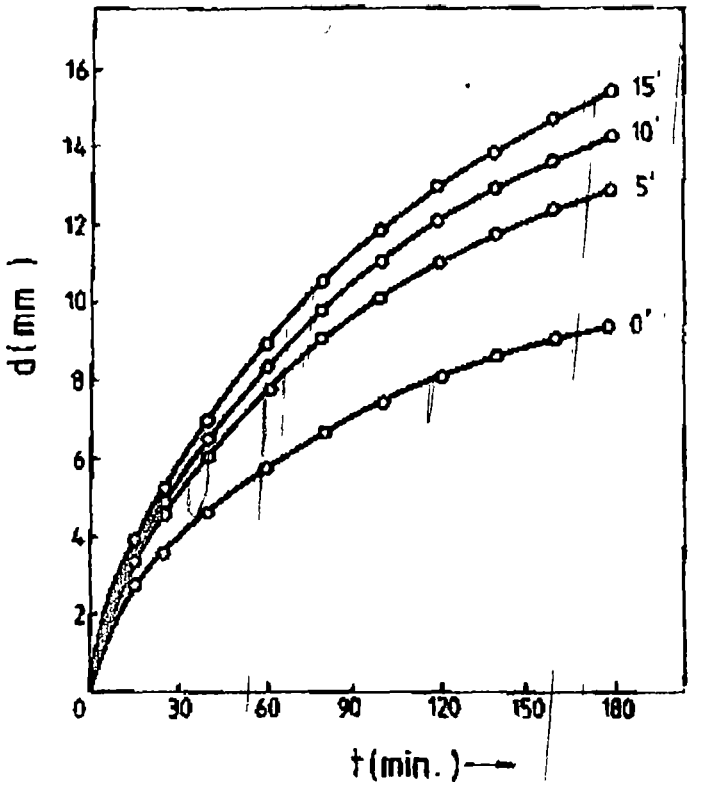

Fig.1. Migration distance of Sr^{2+} in agar gel at different diffusionn times as a function of ultrasonication duration

conductometer, at a temperature of 22° C

The diffusion coefficient was calculated from conductance measurements, as described in [3], using the following formula

$$D = \frac{r^2 \log c_1/c_2}{25(t_2-t_1)}$$

where

c_1 is the concentration of the salt migrated and extracted from the column at time t_1,

c_2 is the concentration measured at time t_2,

r is the radius of the gel column (1 2 mm).

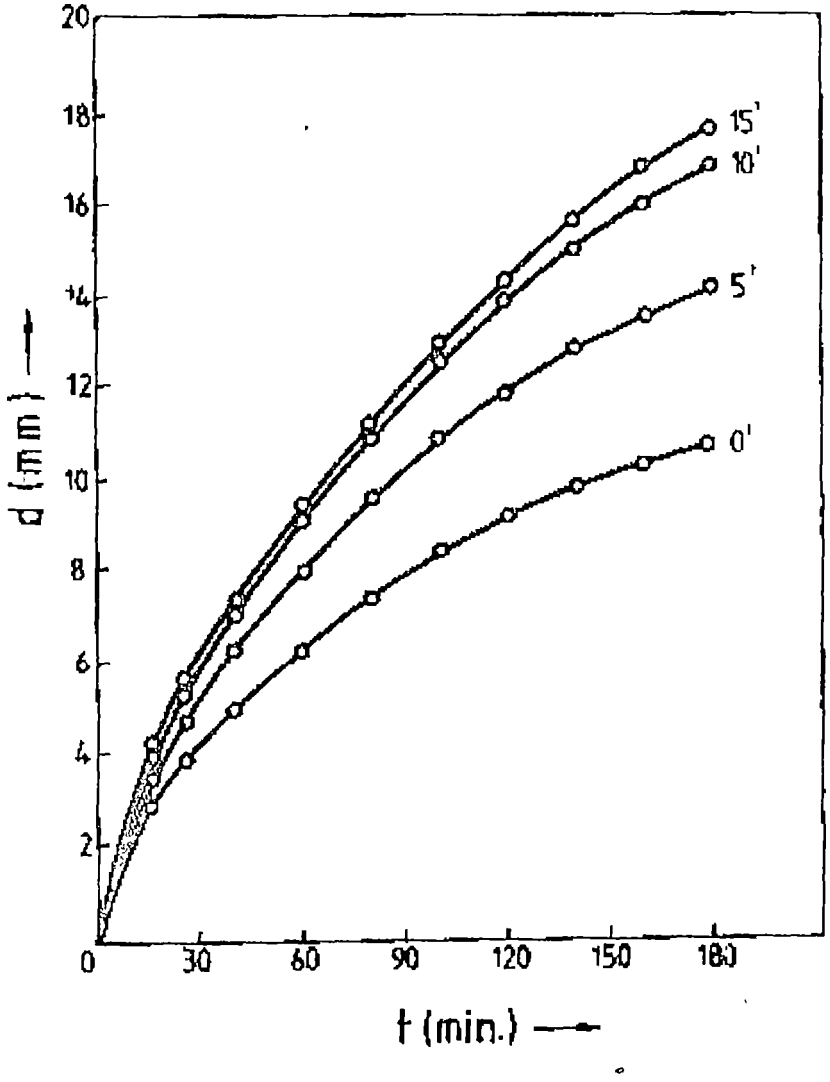

Fig.2. Migration distance of Ba^{2+} in agar gel at different diffusion times as a function of ultrasonication duration

Results. The variation of the effect with the duration of ultrasonication for $SrCl_2$ and $BaCl_2$ solutions is illustrated in Figs 1 and 2 respectively The results of the measurements indicate the increase in the distance travelled by the ions in the gel column as a function of diffusion time, for the three different durations of treatment (5, 10 and 15 min) as compared

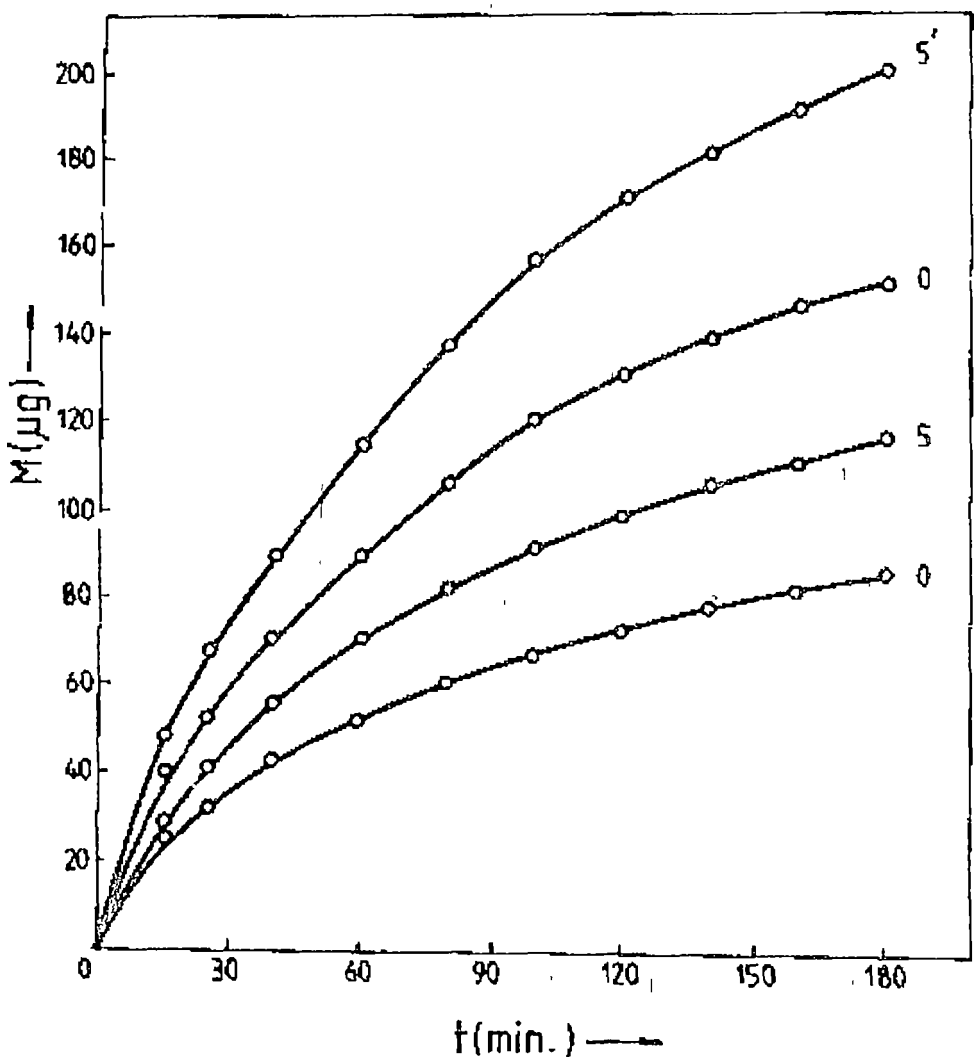

Fig.3. The quantity of ions migrated in agar gel at different diffusion times for $BaCl_2$ solution (upper traces) and $SrCl_2$ solution (lower traces)

to the control There is an initial rapid increase, followed by a slower one, with a tendency to approach an upper limit

The computation results regarding the mass of the diffused ions strengthen even more the above observations, i e the difference between the treated and untreated ions, on one

hand, and between the Sr^{2+} and Ba^{2+} ions, on the other (see Fig 3)

The electric conductance also increases in the solutions treated with ultrasounds as a function of ultrasonication duration, increasing abruptly during the first 10 min of measurement, followed by a slow linear increase (Figs 4 and 5) As can be seen, the absolute values are higher in the case of $BaCl_2$ than $SrCl_2$.

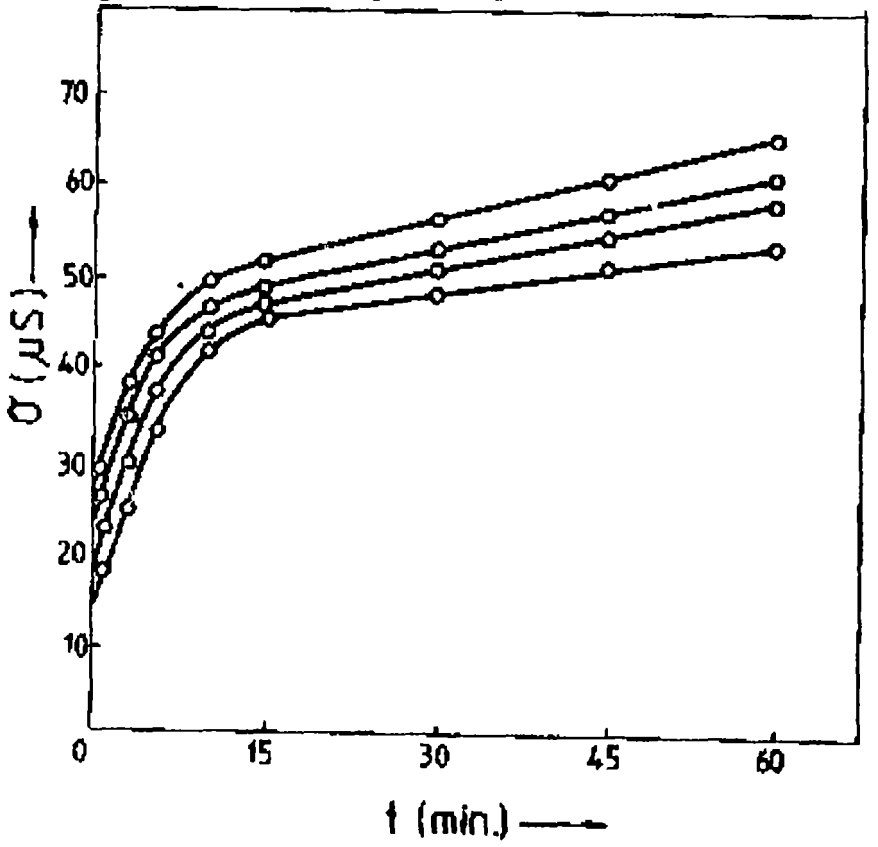

Fig.4. Conductance of $SrCl_2$ solution as a function of time for different durations of ultrasonication

The values of the diffusion constants for the two chloride salts are given in Table 1, for both the control and the 3 durations of ultrasonication

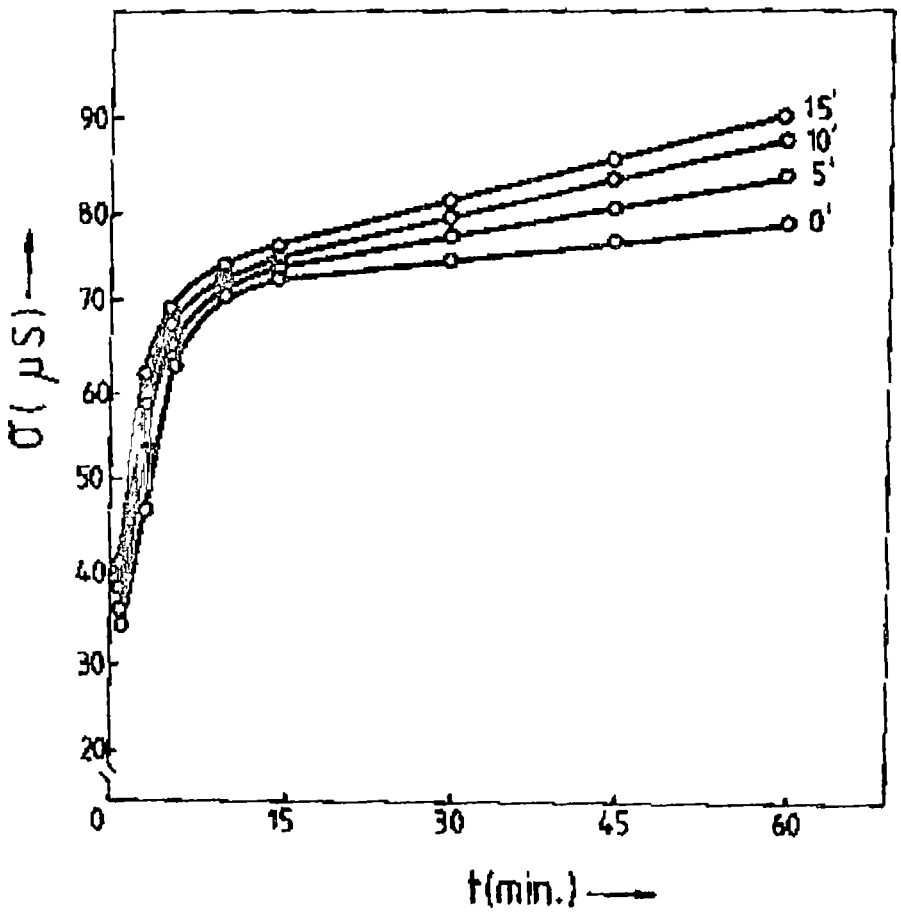

Fig.5. Conductance of $BaCl_2$ solution as a function of time for different durations of ultrasonication

Table 1. - The values of the diffusion constants D for 0 1 N chloride solutions at different durations of ultrasonication

Duration of treatment (min)	$SrCl_2$ D	$BaCl_2$ D
0	1 82	1 92
5	2 34	2 47
10	2 69	2 80
15	2 82	2 91

Again, these values are larger for $BaCl_2$ than for $SrCl_2$

Discussion

The action of ultrasounds on the transport processes is a very debated and still unresolved problem As can be observed also from our experiments, the ultrasound effects are maintained outside the ultrasonic field The mechanical action, the cavitation and its secondary effects, and the radiation pressure are the most important effects that are considered to contribute to the enhancement of the diffusion processes [4,5]

The experiments reported so far in the literature have usually submitted the entire system, or at least the material in which the diffusion takes place, to ultrasonic irradiation Our experiment is the first to show that the effect is preserved even if only the salt solution is treated Since all the measurements indicate a gradual, but saturating effect with increasing durations of sonication, we interprete this as a gradual decrease of the effective radius of the diffusing species, which should result in an increasing value of the diffusion constant, in agrement with Einstein-Stockes law [6]

The most likely explanation of the observed phenomena is the gradual depletion, through ultrasonication, of ion hydratating shells This is supported by the absolute values recorded in the case of the two ions tested Although Ba^{2+} has a larger crystal radius than Sr^{2+} (1 35 A as compared to 1,13 A), its hydrated radius is actually smaller (4 04 A as compared to 4 12 A), a fact which is in agreement with our observations of higher diffusion constants and conductance values for Ba^{2+} This is also in agreement with our previous observation on a series of ultrasonicated solutions of monovalent ions (Li^+, Na^+, K^+) whose behaviour was also consistent with the above interpretation [7]

REFERENCES

1 I Lenart, D Auslander, Ultrasonics, sept , p 216 (1980)
2 E Veress, Proc Int Biophys Congr , Budapest, 234 (1993)
3 Gy Tamás, Gy Rontó, M fiz foly XI, 513 (1963)
4 E Farkas, J Irányi, Az ultrahang, Medicina k Budapest, (1965)
5 M D.Margulis Int Ultrasonic Symp , Wien, 317 (1993)
6 E Chifu, Chimie coloidala Ed Did Ped , Bucuresti, (1969)
7 E Veress, K Pethő, Akusztikai szemle, Bp , 1, 1995 (in print)

STUDIA UNIV BABEŞ-BOLYAI, PHYSICA, XL, 1, 1995

BV QUANTIZATION AND THE FLOW EQUATION

Liviu TĂTARU[1] and Doru BODEA[1]

ABSTRACT. - The Batalin-Vilkovisky formalism provides a useful framework for quantization of gauge theories where the BRST symmetry occurs naturally However in order to obtain the flow equation which describe the evolution of the effective action Γ in the process of varying cutoff Λ, we have to introduce a cutoff, which explicity breaks gauge and hence BRST invariance We derive modified Slavnov-Taylor identities, valid for nonvanishing Λ, which guarantees the BRST invariance of Γ, for $\Lambda\to\infty$ Thus we can study the gauge theories within B-V formalism, by integrating the flow equations

INTRODUCTION The use of flow equations [1] in continuum quantum field theory to simplify proofs of perturbative renormalizability has recently have been task of many investigations In all this papers the flow equations are used to study the dependence of generating functionals on an ultraviolet cutoff Λ or alternatively on an infrared cutoff k The flow equations can be integrated to calculate the Green functions in the limit $\Lambda\to\infty$ (or $k\to 0$) in terms of boundary condition for those functions at some fixed Λ_0 (or k_0)

In both cases the simple form of the flow equations is based on the fact that the cutoff is introduced by modifying the propagators of the fields Thus the challanging problem for the gauge and chiral gauge theories [4] is the fact that local gauge symmetries implemented by BRST symmetries, conflict with the presence of a cutoff However for the SU(2) Yang-Mills theory it was shown in ref [5] that in spite of the explicit breaking of gauge symmetry, the Slavnov-Taylor identities (ST) can be implemented perturbatively by appropriately fixing the boundary conditions

The Batalin-Vilkoviski formalism (BV) encompresses all the ingredients from the Yang-

[1] *"Babeş-Bolyai" University, Faculty of Physics, 3400 Cluj-Napoca, Romania*

Mills theory and can be extended to include more complicated theories involving open algebras and ghosts of ghosts In this short letter we show how the BV formalism can be accomodated for the renormalization group formulation of quantum field theory By using the standard costruction in BV formalism [6] we prove that the validity of Ward or ST identities can be ensured in the limit $k\to 0$ as long as some boundary conditions are fulfilled at some scale k=k' This will be done with the help of modified ST identities

DEVELOPMENT. We begin by a brief review of BV method in a general model of quantum field theory Let $\Phi=\{\Phi^A\}$ denote all fields and ghosts used in the theory and $\Phi^*=\{\Phi^{A^*}\}$ the set of all corresponding anti-fields The anti-field Φ^{A^*} corresponding to the field Φ^A has the opposite statistics and the sum of the ghost numbers of any field and its anti-field is -1 Then they define an action $S=S(\Phi,\Phi^*)$ which should satisfy the master equation

$$(S,S)=0 \tag{1}$$

where (X,Y) is the anti-bracket defined by

$$(X,Y)=\frac{\partial_r X}{\partial\Phi^A}\frac{\partial_l Y}{\partial\Phi^{A^*}}-\frac{\partial_r X}{\partial\Phi^{A^*}}\frac{\partial_r Y}{\partial\Phi^A}=-(-1)^{(\varepsilon_X+1)(\varepsilon_Y+1)}(X,Y)$$

with ε_x the Grassman parity of X In the BV framework we can introduce an aditional term ΔS_k, which will generate an infrared (or ultraviolet) cutoff both for the classical fields and the ghosts It plays the role of the Pauli-Willars regularisation and has the form

$$\Delta S_k=\frac{1}{2}\Phi^A R_{AB}\Phi^B \tag{2}$$

where $R_{AB}(k)$ is a symmetric matrix which does not depend on the fields The total action which is used for the calculation of the generating functional W_k of the connected Green

functions has the form

$$S_\Gamma=S(\Phi,\Phi^*)+\Delta S_K(\Phi) \tag{3}$$

The expression for W_k has the form [HT]

$$Z[J,K]=expiW(J,K)=\int D\Phi expi(S_\Psi(\Phi,\frac{\partial\Psi}{\partial\Phi}+K)+J\Phi) \tag{4}$$

where $\Psi=\Psi(\Phi)$ is the so called gauge fermion, which is needed to fix the gauge, $J=\{J^A\}$ are the usual sources for the fields $\{\Phi^A\}$ and $K=\{K_A\}$ are some aditional sources In the case of the Yang-Mills theory the sources $\{K_A\}$ are completed by the BRST transformations of the fields $\{s\Phi^A\}$ but for a theory with an open algebras this is not the case

Now we use the reprezentation (4) for $W_k(J,K)$ in order to derive the corresponding flow equations In fact we simple have to differentiate both sides of Eq (4) with respect of k and to replace the fields by variations with respect to the corresponding sources, which allows to pull the expresion out of the path integral In this way the flow equation for $Z_k=Z_k(J,K)$ becomes

$$\partial_k Z_k=i(\partial_k R_{AB}(k))\frac{\partial^2 Z_k}{\partial J^A\partial J^B} \tag{5}$$

and for $W_k(J,K)$ one may rewrite as

$$\partial_k W_k=(\partial_k R_{AB}(k))[\frac{\partial W_k}{\partial J^A}\frac{\partial W_k}{\partial J^B}-\frac{\partial^2 W_k}{\partial J^A\partial J^B}] \tag{6}$$

Now we shall derive the modified S-T identities The starting point is the path integral representation of Z_k and the master equation (1) satisfied by the quantum action S We perform a field redefinition

$$\Phi^A\rightarrow\Phi^A+\varepsilon s\Phi^A \tag{7}$$

where

$$sF=(S,F) \tag{8}$$

is the BRST transformation of $F=F(\Phi,\Phi^*)$ and ε is an infinitesimal constant parameter Due to the fact that this local field redefinition does not affect the path integral, we get a condition for the vanishing of a sum of expectation values, which are not manifestly BRST invariant

$$-i\Sigma_k=\langle s(\Delta S_k)+J_A(s\Phi^A)\rangle=0 \tag{9}$$

If one replace fields by variations with respect of sources J^A and K_A, we obtain the following identity for Z_k (modified S-T)

$$\Sigma_k=J^A\frac{\partial lnZ_k}{\partial K^A}+\frac{1}{Z}R_{AB}\frac{\partial^2 Z_k}{\partial J^A\partial J^B}=0 \tag{10}$$

It might happen that the modified S-T identity (10) is satisfied only for some values of k This situation can occur when the quantum action $S=S(\Phi,\Phi^*)$ is modified by some counter terms, but this terms can be chosen by some simple fine tuning equations such that the modified S-T identity (10) is satisfy for some values of k We will not make any reference to their derivation For the values of k where S-T identity is not satisfied i e where $\Sigma_k\neq 0$ we can obtain the k-dependence of it In order to accomplish that we shall calculate the k-derivative of Σ_k

$$\begin{aligned}\partial_k\Sigma_k = &-\frac{1}{2}(\partial_k R_{AB})\frac{1}{Z_k}\frac{\partial^2 Z_k}{\partial J^A\partial J^B}\Sigma_k\\ &+(\partial_k R_{AB})\frac{1}{Z_k}\frac{\partial^2 Z_k}{\partial J^B\partial K^A}\\ &+\frac{1}{2}(\partial_k R_{AB})\langle s(\Delta S_k+J\Phi)\Phi^A\Phi^B\rangle\end{aligned} \tag{11}$$

In order to obtain Eq (11) we have used the definition of Σ_k, Eq (9) and the flow equation (5) Now we can simplify the Eq (11) if we try to rewrite the seccond derivative of Σ_k with respect of J in an convenient form After a straightforward calculation we obtain

$$\frac{\partial^2\Sigma_k}{\partial J^A\partial J^B}=-\frac{2}{Z_k}\frac{\partial Z_k}{\partial J^A}\frac{\partial\Sigma_k}{\partial J^B}+\frac{2}{Z_k}\frac{\partial^2 Z_k}{\partial J^A\partial K^B}-\frac{1}{Z_k}\frac{\partial^2 Z_k}{\partial J^A\partial J^B}\Sigma_k+\langle s(\Delta S_k+J\Phi)\Phi^A\Phi^B\rangle \tag{12}$$

By taking into consideration the equation (12) we can rewrite Eq (11) in the final form, very convenient for the following discussion

$$\partial_k\Sigma_k=(\partial_k R_{AB})(\frac{\partial(lnZ_k)}{\partial J^A}\frac{\partial}{\partial J^B}-\frac{1}{2}\frac{\partial^2}{\partial J^A\partial J^B})\Sigma_k \tag{13}$$

This is the flow equation for Σ_k It represents a linear equation which has a unique solution as long as initial condition $\Sigma_{k=k_0}=\Sigma_0$ is given

REFERENCES

[1] K G Wilson, Phys Rev B4 3174 (1971) K G Wilson and J Kogut, Phys Rep 12, 75 (1974)
[2] J Polchinski, Nucl Phys B231, 269 (1984)
[3] B J Warr, Ann Phys (II) 183 (1988)
[4] C Becchi, "On the construction of renormalized quantum field theory using renormalization group techniques", in "Elementary Particles Field Theory and Statistical Mechanics", Ed M Bonini, G Marchesini, Nucl Phys B409, 441 (1993)
[5] U Ellwanger, Phys Lett. B335, 364 (1994)
[6] J Batalin, G A Vilkovisky, Phys Rev D28 (1983)

STUDIA UNIV. BABEŞ-BOLYAI, PHYSICA, XL, 1, 1995

CHRONICLE

AUGUSTIN MAIOR (1882 -1963) - professor and scientist

God will help you if you learn,
respect and apply the laws of nature
A Maior

Augustin Maior was born on August 24, 1882 in Reghin, a beautiful place in the Eastern part of Transylvania. His parents, Teresa - a well educated and appreciated Christian woman and Gheorghe - teacher and later principal of the local Romanian school, had to grow up five children Olivia, Augustin, Iuliu, Gheorghe and Ana.

Augustin Maior attended the German kindergarten, primary and secondary school in Reghin, the Piarist Lyceum in Targu Mures and the Catholic Lyceum in Budapest. In the last one beside his ability for languages he proved aptitudes for mathematics and physics and succeed to pass his baccalaureate examen in June 1900. Between 1900 and 1904 he attended the courses of the Mechanical Faculty of the Polytechnical Institute in Budapest. During 1905, after graduating from this institute, he participated at special post-graduate courses at famous universities in Vienna, Munich and Göttingen, outstanding scientific personalities like D.Hilbert, H.Minkowski, F.Klein, C.Rünge, E.Riecke, L.Prandtl, E.Wiechert and more youngers M.Born, L.Debyeand and M.von Laue, were teaching at that time.

Starting with November 1905 he was employed at theExperimental Mail station in Budapest where he woned achieve for the first time, the simultaneous transmission of three different conversations on the same line between partners situated at 13 km distance. The theoretical support and experimental proof for such a revolutionary possibility were published in prestigious journals such as "Elektrotechnische Zeitschrift" [1-6] and "The Electrician" [7]

After World Wary, when Transylvania was united with Romania Augustin Maior offered his experience to the new Romanian authorities and was appointed Director of PTT

from Transylvania and Banat in April 14, 1919 In July 1919 he became professor of Physics at the University of Cluj and director of Theoretical and Technological Physics Institute within the Faculty of Science. For more than twenty years he was a permanent fighter for well endowed physics library and laboratories. In 1923 and 1946 A.Maior was the Dean of the Faculty of Science. As professor he offered his students excellent courses, with remarkable modern ideas, that were published in different editions such as "Electricity and Magnetism - 1927 and 1947 and "Acoustics and Optics" - 1932.

Proving to be a great visionary in 1923 he will approve for Hermann Oberth to present his graduation thesis at University of Cluj after having been rejected by Heidelberg University. He will sign the graduation diploma of the scientist who will later be unanimously recognized as the parent of modern interplanetary rackets. As foundes of Theoretical Physics School at the University of Cluj, he maintained permanent contact with the great theoretical physics ideas developed in this period in Europe and he had remarkable personal contributions to these hot fields [8-12]. These contributions were be wonderfully recognized in 1950, when the Nobel Prize laureate M. Louis de Broglie presented A.Maior's paper entitled "Champs gravifique et magnetism"at theAcademy in Paris. This was one of the last happiest events in the dark live of Augustin Maior after 1947 up to 1963 when he died in Cluj.

As an even later recognition of his contribution to the development of modern teaching and research in physics, the council of the Faculty of Physics in the University of Cluj decided in March 1995 that one of the amphitheaters to be named Augustin Maior Amphitheater.

SELECTED PAPERS

1. A.Maior, "Uber Mehrfach-Fernsprechen", Electrotech. Zeitsch., **19**, 84 (1907)
2. A.Maior, "Uber Wechselstrom-Telephonoe", Electrotech. Zeitsch., **47**, 125 (1908)
3. A.Maior, 'Zur Mehrfachtelefonie", Electrotech. Zeitsch.,**38**, 43 (1909)
4. A.Maior, "Die Aussichten der Telephonie und Schnelltelegraphie durch Ozeankabel",

Electrotech. Zeitsch., **15**, 25 (1910)

5. A.Maior, "Telegraphic und Telephonic mit Wechselstršmen auf weite Entfernungen", Electrotech. Zeitsch., **17**, 187 (1912)
6. A.Maior, "Uber das Einschalten langer Leitungen mit Wechselstrom", Electrotech Zeitsch., **21**, 531 (1917)
7. A.Maior, "The use of High-Frequency Alternating Currents in Telegraphy, Telephony and for Power Transmission, The Electrician, **67**, 68 (1914)
8. A Maior, "Temperature et gravitation", Bull de la Soc. de Sciences (Cluj) **2**, 70 (1923)
9. A.Maior, "Energie et radiation dans l'univers en expansion", Bull de la Soc de Sciences (Cluj) **8**, 296 (1935)
10. A.Maior, "Uber Strahlung in Gravitation felde", Physicalishe Zeitch. **18**, 683 (1932)
11. A.Maior, "Sur le champ electromagnetique d'un corps rigide en mouvement", Bull. de la Soc. de Sciences (Cluj) **10**, 312 (1948)
12. A.Maior, "Champ gravitifique et magnetisme" Comptes rendus des séance de l'Academie des Sciences, (Paris) **231**, 607 (1950)

Simion SIMON

In cel de al XL-lea an (1995) *Studia Universitatis Babeş-Bolyai* apare în următoarele serii:

matematică (trimestrial)
fizică (semestrial)
chimie (semestrial)
geologie (semestrial)
geografie (semestrial)
biologie (semestrial)
filozofie (semestrial)
sociologie-politologie (semestrial)
psihologie-pedagogie (semestrial)
ştiinţe economice (semestrial)
ştiinţe juridice (semestrial)
istorie (semestrial)
filologie (trimestrial)
teologie ortodoxă (semestrial)
educaţie fizică (semestrial)

In the XL-th year of its publication (1995) *Studia Universitatis Babeş-Bolyai* is issued in the following series:

mathematics (quarterly)
physics (semesterily)
chemistry (semesterily)
geology (semesterily)
geography (semesterily)
biology (semesterily)
philosophy (semesterily)
sociology-politology (semesterily)
psychology-pedagogy (semesterily)
economic sciences (semesterily)
juridical sciences (semesterily)
history (semesterily)
philology (quarterly)
orthodox theology (semesterily)
physical training (semesterily)

Dans sa XL-e année (1995) *Studia Universitatis Babeş-Bolyai* paraît dans les series suivantes:

mathematiques (trimestriellement)
physique (semestriellement)
chimie (semestriellement)
géologie (semestriellement)
géographie (semestriellement)
biologie (semestriellement)
philosophie (semestriellement)
sociologie-politologie (semestriellement)
psyhologie-pédagogie (semestriellement)
sciences économiques (semestriellement)
sciences juridiques (semestriellement)
histoire (semestriellement)
philologie (trimestriellement)
théologie orthodoxe (semestriellement)
éducation physique (semestriellement)

CONTENTS